

Article

On the Parametrization of Epidemiologic Models—Lessons from Modelling COVID-19 Epidemic

Yuri Kheifetz , Holger Kirsten  and Markus Scholz 

Institute for Medical Informatics, Statistics and Epidemiology, University of Leipzig, Haertelstrasse 16-18, 04107 Leipzig, Germany; holger.kirsten@imise.uni-leipzig.de

* Correspondence: yuri.kheifetz@imise.uni-leipzig.de (Y.K.); markus.scholz@imise.uni-leipzig.de (M.S.); Tel.: +49-341-97-16348 (Y.K.); +49-341-97-16190 (M.S.)

Abstract: Numerous prediction models of SARS-CoV-2 pandemic were proposed in the past. Unknown parameters of these models are often estimated based on observational data. However, lag in case-reporting, changing testing policy or incompleteness of data lead to biased estimates. Moreover, parametrization is time-dependent due to changing age-structures, emerging virus variants, non-pharmaceutical interventions, and vaccination programs. To cover these aspects, we propose a principled approach to parametrize a SIR-type epidemiologic model by embedding it as a hidden layer into an input-output non-linear dynamical system (IO-NLDS). Observable data are coupled to hidden states of the model by appropriate data models considering possible biases of the data. This includes data issues such as known delays or biases in reporting. We estimate model parameters including their time-dependence by a Bayesian knowledge synthesis process considering parameter ranges derived from external studies as prior information. We applied this approach on a specific SIR-type model and data of Germany and Saxony demonstrating good prediction performances. Our approach can estimate and compare the relative effectiveness of non-pharmaceutical interventions and provide scenarios of the future course of the epidemic under specified conditions. It can be translated to other data sets, i.e., other countries and other SIR-type models.

Keywords: COVID-19 epidemiologic models; parametrization; extended multi-compartment SIR-type model; input-output non-linear dynamical system; Bayesian knowledge synthesis



Citation: Kheifetz, Y.; Kirsten, H.; Scholz, M. On the Parametrization of Epidemiologic Models—Lessons from Modelling COVID-19 Epidemic. *Viruses* **2022**, *14*, 1468. <https://doi.org/10.3390/v14071468>

Academic Editors: Thanasis Fokas and George Kastis

Received: 11 May 2022

Accepted: 29 June 2022

Published: 2 July 2022

Publisher's Note: MDPI stays neutral with regard to jurisdictional claims in published maps and institutional affiliations.



Copyright: © 2022 by the authors. Licensee MDPI, Basel, Switzerland. This article is an open access article distributed under the terms and conditions of the Creative Commons Attribution (CC BY) license (<https://creativecommons.org/licenses/by/4.0/>).

1. Introduction

Predicting the spread of an infectious disease is a pressing need as demonstrated for the present SARS-CoV-2 pandemic. Due to the worldwide high disease burden, a plethora of mathematical epidemiologic models was proposed. This includes auto-regressive time series methods, Bayesian techniques, and application of deep learning methods, but also mechanistic models and hybrid models combining some of these approaches (see [1] for a review). Among mechanistic models, based either on agents [2–4] or on compartments [5], the most commonly proposed and published model type is the classical SIR (S = susceptible, I = infected, R = recovered) type compartment model, which was presented with different modifications often considering further aspects and details such as disease states, age structure, contact patterns, and intervention effects. Major aims of these models are to predict (1) the dynamics of infected subjects, (2) requirements of medical resources during the course of the epidemic, or (3) the effectiveness of non-pharmaceutical intervention programs (NPI) [6,7]. Examples for models addressing these aims are a SECIR model (E = exposed, C = cases) proposed by Khailaie et al. [8], a SEIR type model proposed by Barbarossa et al. [9], models from The Robert-Koch institute [10], and from Dehning et al. [11].

A good prediction performance does not only depend on the precise structure of the model but on its parametrization. This, however, is a non-trivial and often underestimated task due to the following issues applicable to other infectious diseases as well:

key epidemiologic parameters are often unknown or only known within ranges. Therefore, parametrization based on observational data is a common approach. However, reported official data bases are heterogeneous and often biased due to (1) lag in reporting of cases/events [12], (2) changing testing policy either due to limited testing capacities, which might depend on the pandemic situation itself or by changing risk profiles of people to be tested (e.g., defined risk groups, dependence on symptoms, degree of prophylactic testing) [13], and (3) incompleteness of data [14]. Moreover, parametrization depends on further epidemiologic issues to be considered, comprising (1) changing age-structure of the infected population with impact on symptomatology, hospital or intensive care requirements and mortality, (2) spatial heterogeneity of the spread of the disease driven by local conditions and outbreaks, (3) new pathogen variants becoming prevalent, (4) non-pharmaceutical interventions continuously updated in response to the pandemic situation, and finally, (5) the progress of vaccination programs and its effectiveness.

Due to these interacting complexities, it is close to impossible to construct a fully mechanistic model covering all these aspects in parallel. Therefore, we here propose a framework of epidemiologic model parametrization, which accounts for these issues in a more phenomenological, data-driven way applicable even for limited or biased data resources.

In detail, we here propose to integrate a mechanistic epidemiologic model as a hidden layer into an input-output non-linear dynamical system (IO-NLDS), i.e., the true epidemiologic dynamics cannot be directly observed. This allows distinguishing between features explicitly modelled (in our case different virus variants, vaccination) and changing factors of the system which are difficult to model mechanistically (in our case changes of contacts, e.g., due to non-pharmaceutical interventions or changing contact behavior, changing age-structure of the infected population and changes in testing policy, in the following abbreviated as NPI/behavior). These factors are imposed as external inputs of the system.

We then estimate parameters by a knowledge synthesis process considering prior information of parameter ranges derived from different external studies and other available data resources such as public data. We are thus going beyond previous modeling approaches that only used point estimates for parameters [15,16]. Specifically, we use Bayesian inference for the parameter estimation, which could also be time-dependent. We analyze the structure of available public data in detail and translate it to model outputs linked by an appropriate data model to the hidden states of the IO-NLDS, i.e., the epidemiologic model. We demonstrate this approach on an example epidemiologic model of SECIR type for SARS-CoV-2 and data of Germany and Saxony, but our method can be translated to other countries, other models or even other infectious disease contexts.

2. Materials and Methods

2.1. General Approach

We consider input-output non-linear dynamical systems (IO-NLDS) originally proposed as time-discrete alternatives to physiological pharmacokinetic and –dynamics differential equations models [17]. This class of models couples a set of input parameters such as external influences and factors with a set of output parameters, i.e., observations by a hidden model structure to be learned (named *core model* in the following). This coupling is not necessarily fully deterministic, i.e., data are not required to represent directly state parameters of the model. This represents a major feature of our approach in order to account for different types of biases in available observational time series data.

We here demonstrate our approach by using an epidemiological model as core of the IO-NLDS. Non-pharmaceutical interventions, changes of testing policy, age distributions and severity of disease courses were phenomenologically modelled by external control parameters imposed on the epidemiologic model via the input layer of the IO-NLDS. Random influxes of infected subjects e.g., by travelling activities or outbreaks are also considered by this approach. Number of reported infections, intensive care (IC) cases, and deaths are considered as output parameters not directly representing the hidden states of

the model due to several data issues including reporting delays. The model is then fitted to data by a full information approach, i.e., all data points were evaluated by a suitable likelihood function.

The single steps of this process are explained in detail below.

Assumptions of the core model

We adapted a standard SECIR model (SECIR = susceptible, exposed, cases, infectious, recovered) for pandemic spread. We introduced an asymptomatic compartment in order to account for infected patients, which do not have symptoms, a common condition of SARS-CoV-2 infection. A compartment of patients requiring intensive care (IC) was added to model respective requirements and we distinguished between deceased and recovered patients.

We subdivided most of the compartments into three sub-compartments with first order transitions to model time delays. Transition rates between sub-compartments are the same for each respective compartments for the sake of parsimony. This approach is extensively used in pharmacological models [10]; it is equivalent to a Gamma-distributed transit time [11]. To allow for two concurrent virus variants with differing properties, compartments of asymptomatic and symptomatic infected subjects are duplicated. This allows us, for example, to simulate the take-over of the more infectious B.1.1.7 (Alpha), and later, B.1.617.2 (Delta) variant observed e.g., in all European countries [12].

The general scheme of the IO-NLDS system is shown in Figure 1. We make the following assumptions:

1. The input layer consists of external modifiers influencing (1) reporting policy (e.g., changing testing policy), (2) rates of infections (affected by non-pharmaceutical interventions, age structure, influx of cases), and (3) risks of severe disease conditions such as IC requirements and deaths, also depending on the changing age structure of infected subjects.
2. The output layer of observable data is linked to the hidden layers of the core model by specific data models (see later).
3. Susceptible, non-infected people (S_c): We assume that 100% of the population is susceptible to infection at the beginning of the epidemic.
4. The latent state E comprises infected but non-infectious people.
5. The asymptomatic infected state I_A has three sub-compartments ($I_{(A,1)}$, $I_{(A,2)}$ and $I_{(A,3)}$). From $I_{(A,1)}$, transitions to the symptomatic state or the second asymptomatic state are possible. From $I_{(A,2)}$, only transitions to $I_{(A,3)}$ and then to the recovered state R are assumed.
6. The symptomatic infected state I_S is also divided into three compartments ($I_{(S,1)}$, $I_{(S,2)}$, and $I_{(S,3)}$). The sub-compartment $I_{(S,1)}$ comprises an efflux toward the sub-compartment C_1 representing deteriorations toward critical disease states. Otherwise, the patient transits to $I_{(S,2)}$. From $I_{(S,2)}$, a patient can either die representing deaths without prior intensive care or transit to $I_{(S,3)}$. Finally, the efflux of $I_{(S,3)}$ flows into R representing resolved disease courses.
7. Both cases I_A and I_S contribute to new infections but with different rates to account for differences in infectivity and quarantine probabilities.
8. The compartment C represents critical disease states requiring intensive care. We assume that these patients are not infectious due to isolation. Again, the compartment is divided into three sub-compartments, C_1 , C_2 , and C_3 . In C_1 , a patient can either die or transit to C_2 , C_3 , and finally, R .
9. Patients on the recovered stage R are assumed to be immune against re-infections.
10. We duplicate the compartments E , $I_{(A,1)}$, \dots , $I_{(A,3)}$, $I_{(S,1)}$, \dots , $I_{(S,3)}$ to account for two concurrent virus variants. We assume different infectivities for the two variants. All other parameters are assumed equal. No co-infections are assumed.

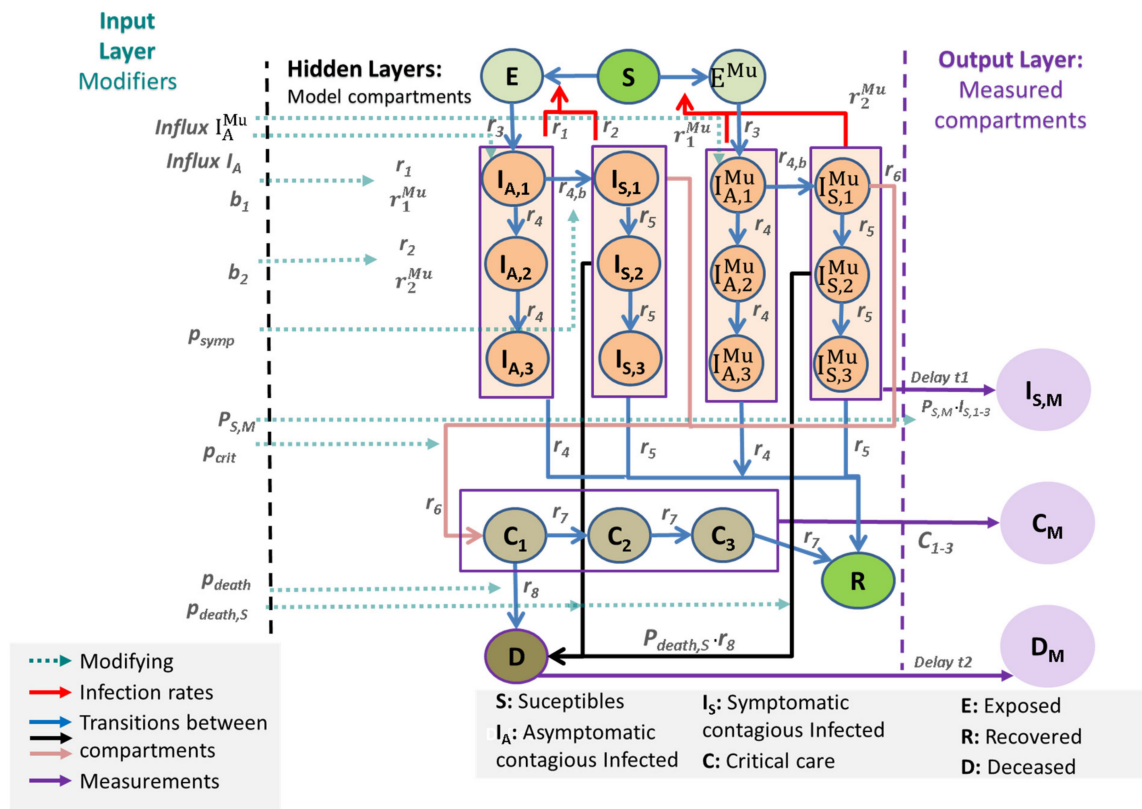


Figure 1. General scheme of our IO-NLDS model. The epidemiologic SEICIR model is integrated as a hidden layer. Respective equations are provided in Appendix A. The input layer consists of external modifiers including parameter changes due to changes in testing policy, non-pharmaceutical interventions, and age-structures. The output layer is derived from respective hidden layers via stochastic relationships (see later). The output layer is compared with real-world data. The superscript Mu denotes new virus variants.

These assumptions are translated into a difference equation system (see Appendix A). Model compartments and their properties are explained in Table 1.

Table 1. Description of model compartments. We describe the compartments of the model and their biological meaning. Compartments E, I_A , and I_S are duplicated to account for two concurrent virus variants.

Compartment Name	Sub-Compartments	Description
S_c		Susceptible
E		Latent stage (not infectious)
I_A	$I_{A,1}$	Asymptomatic infected state 1, can either develop symptoms, i.e., transit to $I_{S,1}$ with probability p_{symp} and rate r_{4b} or stays asymptomatic with probability $1 - p_{symp}$ and transits to $I_{A,2}$ with rate r_4
	$I_{A,2}$	Asymptomatic infected state 2, transits to $I_{A,3}$ with rate r_4
	$I_{A,3}$	Asymptomatic infected stage 3 transits to R with rate r_4
I_S	$I_{S,1}$	Symptomatic infected state 1. Can either become critical, i.e., transits to C_1 with probability p_{crit} and rate r_6 or stays sub-critical with probability $1 - p_{crit}$ and transits to $I_{S,2}$ with rate r_5

Table 1. Cont.

Compartment Name	Sub-Compartments	Description
C	$I_{S,2}$	Symptomatic infected state 2, can either die, i.e., transits to D with probability $p_{death,S}$ or transits to $I_{S,3}$ with probability $(1 - p_{death,S})$ and rate r_5
	$I_{S,3}$	Symptomatic infected state 3, transits to R with rate r_5
	C_1	Critical state 1, not infectious. Can either die, i.e., transits to D with probability p_{death} and transit rate r_8 or stays critical with probability $1 - p_{death}$ and transits to C_2 with rate r_7
	C_2	Critical state 2, transits to C_3 with rate r_7
	C_3	Critical state 3, transits to R with rate r_7
R		Recovered (absorbing state)
D		Dead (absorbing state)

All model parameters of the model are described in Table 2. Complete dynamics of the epidemic in Germany is shown in Figures 2 and 3.

Table 2. Basic model parameters. We present prior values and ranges derived from the literature as well as estimated values derived from parameter fitting. Transit rate means reverse of transit time of the respective compartment. Posteriors can be found in Figure 4. §: Further details and definitions on parameters are given in the Appendix A Equations (A1) and (A2), where also a justification of priors is provided, (Appendix H).

Parameter	Unit	Description	Source	Reference	Value	Prior Mean	Min	Max
influx	Subjects per day	Initial influx of infections into compartment E until first interventions	Estimated	§	3171	-	-	-
r_1	Day ⁻¹	Infection rate through asymptomatic subjects	Estimated	§	1.19	-	-	-
r_2	Day ⁻¹	Infection rate through symptomatic subjects	Set equal to $rb_{1,2} \cdot r_1$ (parsimony)	§	0.451	-	-	-
$rb_{1,2}$	-	Proportion of infection rate symptomatics/asymptomatics r_1/r_2	Estimated	§	0.379	-	0	-
r_3	Day ⁻¹	Transit rate for compartment E (latent time)	prior constraint	§, [10,18–21]	0.272	1/3	1/4	1/2
r_4	Day ⁻¹	Transit rate for asymptomatic sub-compartments	prior constraint	§,[22–25]	0.636	3/5	3/10	3/4
$r_{4,b}$	Day ⁻¹	Rate of development of symptoms after infection	prior constraint	§, [10,18–21,26–28]	0.456	2/55	1/5	1
r_5	Day ⁻¹	Transit rate for symptomatic sub-compartments	prior constraint	§	0.946	6/5	6/15	6/3
r_6	Day ⁻¹	Rate of development of critical state after being symptomatic	prior constraint	§, [10,29–31]	0.186	1/5	1/7	1/4

Table 2. Cont.

Parameter	Unit	Description	Source	Reference	Value	Prior Mean	Min	Max
r_7	Day ⁻¹	Transit rate for critical state sub-compartment	prior constraint	§,[10,32–34]	0.159	3/17	3/35	3/8
r_8	Day ⁻¹	Death rate of patients in critical sub-compartment 1	prior constraint	§, [29,35,36]	0.104	1/8	1/14	2/13
p_{symp}	-	Probability of symptoms development after being infected	Set or prior constrained (overfitted if estimated unconstrained)	§,[37–39]	0.5	-	0.3	0.8
p_{crit} ($p_{crit,0}$)	-	Initial value $p_{crit,0}$ of step function p_{crit} , the probability of becoming critical after developing symptoms	Estimated	§, [9,27]	0.0765	-	0	1
p_{death} ($p_{death,0}$)	-	Initial value $p_{death,0}$ of step function p_{crit} , the probability of dying after becoming critical	Estimated	§, [32]	0.119	-	0	1
$p_{death,S}$	-	Probability of death after developing symptoms without becoming critical	Set equal to $p_{death,S,0} \cdot p_{death}$ (parsimony)	§, [32]	-	-	0	1
$p_{death,S,0}$	-	Proportionality factor for probability of death after developing symptoms without becoming critical	Estimated	§	0.587	-	-	-
$P_{S,M}$	-	Fraction of unreported cases	prior constraint	§, [40,41]	0.499	0.5	0.1	0.90
mur	-	Ratio of $r1^{Mu}/r1 = r2^{Mu}/r2$ reflecting higher infectivity of B.1.1.7 variant	Set	§	1.65	-	-	-

2.2. Input Layer

The input layer represents external factors acting at the SECIR model, effectively changing its parameters [42]. We define step functions b_1 and b_2 as time-dependent input parameters modifying the rate of infections caused by asymptomatic, respectively symptomatic subjects. To identify dates of change, we used a data-driven approach based on a Bayesian Information Criterion informed by changes in non-pharmaceutical interventions for Germany based on Government decisions, changing testing policies as well as events with impact on epidemiological dynamics such as holidays or sudden outbreaks. Details can be found in Appendix B.

We also accounted for changes in the probabilities of critical courses and mortality, which can be explained by changes in testing policies covering asymptomatic cases to a different extent (for example symptomatic testing only vs. introduction of screening tests, e.g., rapid antigen tests), respectively shifts in the age-distribution of patients or changes in patient care efficacy (new pharmaceutical treatment, overstretched medical resources). Again, this is implemented by step functions p_{crit} , respectively p_{death} . Number of steps are determined on the basis of a Bayesian Information Criterion. Details can be found in the Appendix B as well as in Table A5 from Appendix I and Table A8 from Appendix J.

The parameter $P_{S,M}$ represents the percentage of reported infected symptomatic subjects in relation to all symptomatic subjects. This value is assumed to be constant (50%) in the present version of the model. We describe the parameters defining the input layer in Table 3.

Table 3. Parameters used to define the input layer. These parameters were used to empirically model changing NPIs or changing contact behavior, changes in testing policies and changing age-structures during the course of the epidemic. Respective input functions constitute the input layer of our IO-NLDS model.

Parameter	Unit	Description	Source	Remarks
N_{tr}	-	Number of time points of changes of NPI/contact behavior	Empirically defined	13 intensifications, 15 relaxations identified (determined by information criterion)
$b_{tr,j}, j = 1, \dots, N_{tr}$	-	Relative infectivity of subjects in the time interval $[tr, tr + 1]$	Estimated	assumed to be the same for symptomatic and asymptomatic patients
$Tr_j, j = 1, \dots, N_{tr}$	Days	Time points of NPI/contact behavior changes	Estimated or fixed	Strictly monotone sequence
N_{crit}	-	Number of time steps of $p_{crit}(t)$	Empirically defined	18 (determined by information criterion)
$\alpha_{crit,j}, j = 1, \dots, N_{crit}$	-	Value of p_{crit} between two time steps	Estimated	Within the interval $[0, 1]$
$T_{p_{crit},j}, j = 1, \dots, N_{crit}$	Days	Time points of changes of p_{crit}	Estimated	Strictly monotone sequence
N_{death}	-	Number of time steps of $p_{death}(t)$	Empirically defined	19 (determined by information criterion)
$\alpha_{death,j}, j = 1, \dots, N_{death}$	-	Value of p_{death} between two time steps	Estimated	Within the interval $[0, 1]$
$T_{p_{death},j}, j = 1, \dots, N_{death}$	Days	Time points of changes of $p_{death}(t)$	Estimated	Strictly monotone sequence
Del_{tr}	Days	Delay of activation of NPI	Fixed	2 days

2.3. Output Layer and Data

We fit our model to time series data of reported numbers of infections $I_{S,M}$, deaths D_M , and occupation of ICU beds C_M representing the output layer of our IO-NLDS model. Data source of infections and deaths were official reports of the Robert-Koch-Institute (RKI) in between 4 March 2020 and 29 March 2021. Number of critical cases were retrieved from the German Interdisciplinary Association of Intensive and Emergency Medicine (Deutsche Interdisziplinäre Vereinigung für Intensiv- und Notfallmedizin e.V.—DIVI) in between 25 March 2020 and 29 March 2021. Time points in proximity to Christmas and the turn of the year (19 December 2020 to 19 January 2021) were heavily biased and therefore omitted during parameter fitting.

However, also for the considered time intervals several sources of bias need to be considered. We handled these issues as explained in the following:

Infected cases: We first smoothed reported numbers of infections with a sliding window of seven days centered on the time point of interest to control for strong weekly periodicity. We assume that these numbers correspond to a certain percentage $P_{S,M}$ of symptomatic patients. This is justified by the fact that the majority of reported infected cases develop symptoms (about 85% according to the RKI [43]), but there is also a large amount of asymptomatic cases (approximately 55–85% of infections [37–39]). In the present model, we assume $P_{S,M}$ as constant. The exact equation linking states of the SECIR model with the measured numbers of infected subjects $I_{S,M}$ can be found in Appendices B and C Equation (A7). We further accounted for delays in the reporting of case numbers by introducing a log-normally distributed delay time as explained in Appendix C.

Critical cases: The number of critical COVID-19 cases (DIVI reported ICU) is available since end of March 2020 [44]. We assumed that these data are complete since 16 April 2020 when reporting became mandatory by law in Germany. Earlier data were up-scaled from the number of reporting hospitals to the number of ICU-beds of all hospitals according to the reported ICU capacity available for 2018. We coupled the sum of the critical sub-compartments C_i ($i = 1,2,3$) to these numbers directly.

Deaths: Deaths are reported by the RKI but daily reports do not reflect true death dates, which needs to be accounted for. Available daily death data of the RKI are retrospectively updated with a delay between true death date and reported date (death report delay—DRD). We assume that the DRD is normally distributed with an average of 7.14 days and a standard deviation of 4 days as reported by Delgado et al. [45]. Details can be found in Appendix C.

Occurrence of B.1.1.7 variant: In January 2021, the variant B.1.1.7 became endemic in Germany and quickly replaced all other variants. Onset of this development was modeled by an instantaneous influx of 5% of newly infected subjects into the E^{Mu} compartment on 26 January 2021 estimated from published data [46].

2.4. Parametrization

We carefully searched the literature to establish ranges for our model parameters. These ranges are used as prior constraints during parametrization of our model (Table 2). Justification of prior values is provided in Appendix H. Parameters are then derived by fitting the predictions of the model to reported data of infected subjects, ICU occupation, and deaths using the link functions of model and data explained in the previous section. This is achieved via likelihood optimization. Likelihood is constructed using the same principles as reported [47]. In short, the likelihood consists of three major parts, namely the likelihood of deviations from prior values, the likelihood of residual deviations from the data, and a penalty term to ensure that model parameters are within the prescribed ranges, as explained in Appendix D. We follow a full-information approach intended to use all data collected during the epidemic as explained in Appendices E–G. As a result, our model fits well to the complete dynamics of the epidemic in Germany in the above mentioned time period (Figures 2 and 3).

To ensure identifiability of parameters, we checked a number of parsimony assumptions. For example, we assumed that the dynamical infection intensities of asymptomatic ($b_1 \cdot r_1(t)$) and symptomatic subjects ($b_2 \cdot r_2(t)$) are proportional with factor $rb_{1,2}$. We also determined Bayesian Information criteria (BIC) for different partitioning numbers of the external jump functions (N_{crit} and N_{death}) to keep these as small as possible. Details can be found in Appendix B.

Likelihood optimization is achieved using a stochastic approximation of an estimation-maximization algorithm (SAEM) [48]. The algorithm is based on a stochastic integration of marginal probabilities without using likelihood approximations such as linearization or quadrature approximation or sigma-point filtering [17].

Confidence intervals of model predictions are derived by Markov-Chain-Monte-Carlo simulations, i.e., alternative parameter settings were sampled from the parameter space around the optimal solution (Appendices B, F and G). We use these parameter sets to simulate alternative epidemic dynamics. This resulted in a distribution of model predictions from which empirical confidence intervals are derived.

2.5. Implementation

The model and respective parameter estimations are implemented in the statistical software package R from which external publicly available functions are called. The model's equation solver is implemented as C++ routine and called from R code using the Rcpp package. The code and data for simulation of the output layers using the reported parameter settings will be made available via our Leipzig Health Atlas: (<https://www.>

health-atlas.de/models/40, accessed on 26 June 2022) and GitHub (<https://github.com/GenStatLeipzig/LeipzigIMISE-SECIR>, accessed on 26 June 2022) [49].

3. Results

3.1. Explanation of Epidemiologic Dynamics

We used the full data set to explain the course of infections, ICU occupations, and deaths between 4 March 2020 and 29 March 2021 in Germany. A total of three parameters were assumed time-dependently, namely Infectivity b_1 and the probability of a critical disease course (p_{crit}) and death (p_{death}). We identified nine fixed and 19 empirically identified time points of NPI/behavioral changes (Table A1 from Appendix I). Regarding p_{crit} and p_{death} , we identified 18 respectively 19 time steps (See Tables A2 and A3 from Appendix I and Table A7 from Appendix J). Throughout the epidemic, we observed a good agreement of our model and incident (Figure 2) and cumulative data (Figure 3). Corresponding residual errors are provided for all observables (Table A4 from Appendix I). As shown in Table A2 from Appendix I, we estimated 14 static and three dynamically changing parameters using 1170 data points (390 daily measurements of registered cases, registered deaths and ICU occupancy) for Saxony as well as for Germany.

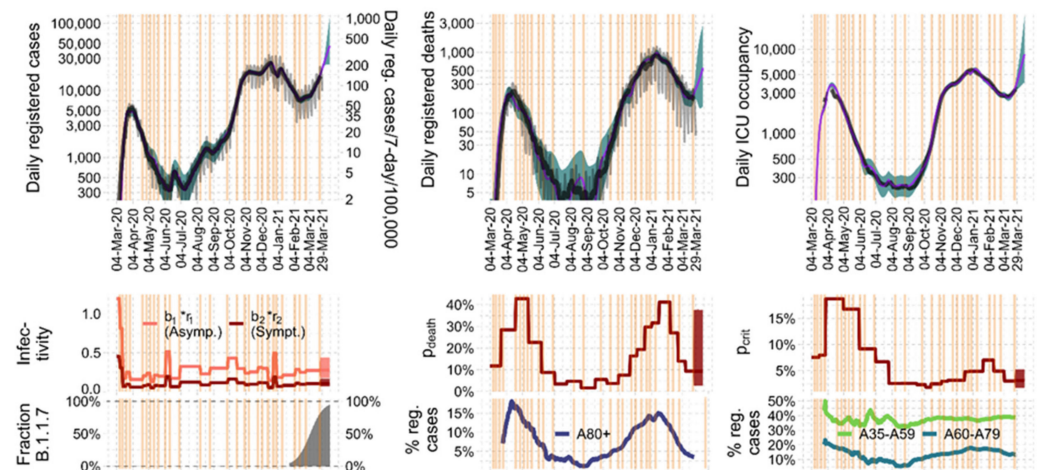


Figure 2. Agreement of model and incident data. We show incident infections, deaths, and daily ICU occupancy during the course of the epidemic in Germany in between 4 March 2020 and 29 March 2021. Comparison of IO-NLDS model (magenta curve) and data (thin grey curves = raw data, solid black curve = data averaged by sliding window) is provided in the upper column. A good agreement is observed (shaded area = prediction uncertainty, vertical lines = changes in NPI/contact behavior). The middle row represents the corresponding input layer, i.e., the estimated time course of the time-dependent input parameters, namely infectivity and probabilities of critical disease course and death. Time steps correspond to the lines of changing NPI/contact behavior as displayed in the upper row. In the lower row, we present percentages of B.1.1.7 among infected subjects (first figure), subjects older than 80 years among infected corresponding to high death tolls (second), and subjects in the age categories 35–59, respectively 60–79 among critical cases (last figure of last row).

3.2. Parameter Estimates and Identifiability

Parameter estimates of the SECIR model are presented in Table 2, while those required to define the input layer are presented in Table 3 and Tables A1 and A3 from Appendix I. For those parameters for which we used prior information for fitting purposes, we compared the respective expected posteriors with their best priors (see Figure 4). Statistics are provided in Table A5 from Appendix I. No significant deviations between expected values of posteriors and priors were detected. All relative errors of parameters of the SECIR model are smaller than 10% demonstrating excellent identifiability of all epidemiologic parameters. As expected, identifiability of the external control functions is reduced. Largest

standard errors of steps are in the order of 70% still demonstrating reasonable identifiability (Table A3 from Appendix I).

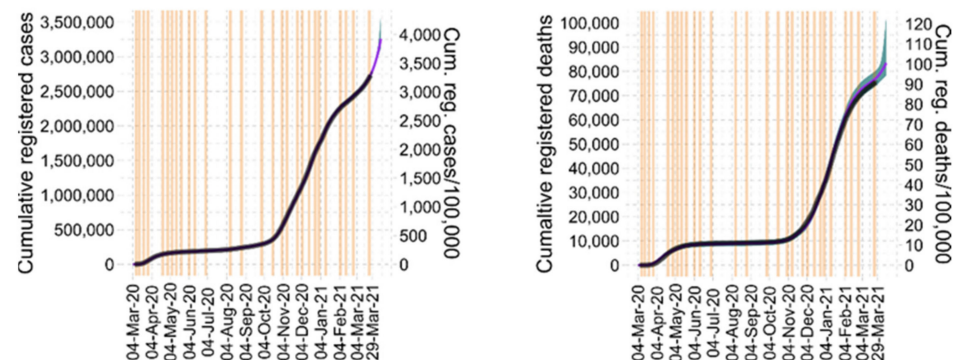


Figure 3. Agreement of model and cumulative data. We show cumulative infections and deaths during the course of the epidemic in Germany in between 4 March 2020 and 29 March 2021. Comparison of IO-NLDS model (magenta curve) and data (solid black curve) is provided. A good agreement is observed (shaded area = prediction uncertainty, vertical lines = changes in NPIs/contact behavior).

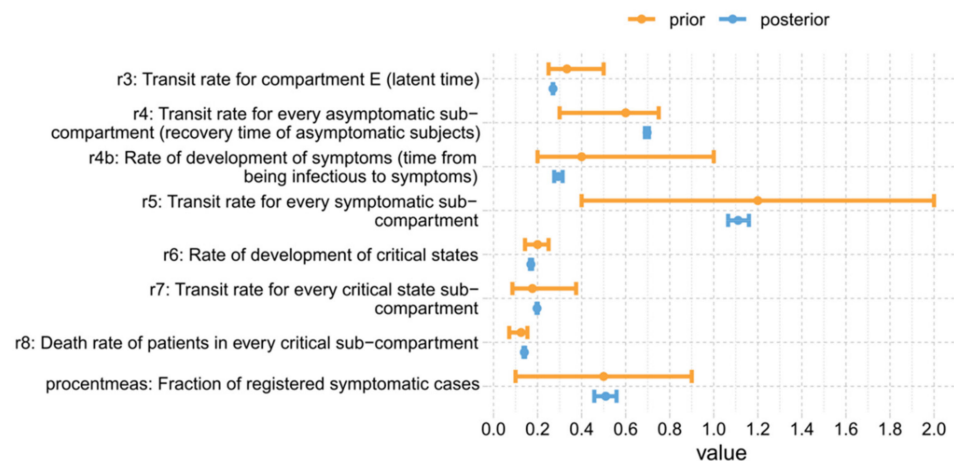


Figure 4. Comparison of prior and posterior values of estimated parameters of the SECIR model. We present prior vs. posterior distributions of estimated parameters of the SECIR model. Ranges for priors represent assumed minimum and maximum values. Ranges for posteriors represent 95%-confidence intervals. Numbers are provided in Table A8 from Appendix J.

3.3. Plausibilization of Estimated Step Functions of Infectivity

We estimated the infectivity as an empirical step function through the course of the epidemic. This step function should also roughly reflect NPI effectivity. We therefore compared our infectivity step function with the Governmental stringency index of NPI as estimated on the basis of Hale et al. [50]. Results are displayed at Figure 5 and revealed a reasonable agreement.

3.4. Model Predictions

We regularly used our model to make predictions regarding the future course of the epidemic. Predictions were specifically made for the Free State of Saxony, a federal state of Germany and were published at the Leipzig Health Atlas [49]. We here present comparisons of our predictions with the actual course of the epidemic for two scenarios to demonstrate utility of our approach. Parameter values for Saxony were obtained in the same way as for Germany restricting available data of infected subjects, ICU cases, and deaths to this state. Estimated parameter values are presented in Tables A6–A8 from Appendix J.

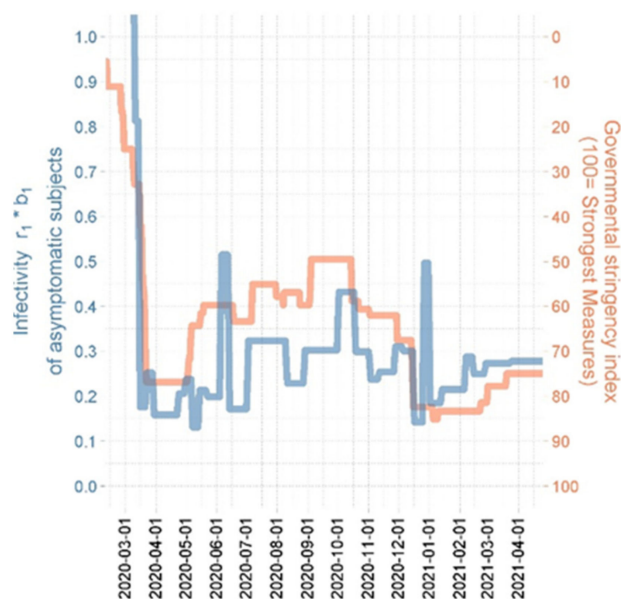


Figure 5. Relationship between estimated step function of infectivity of asymptomatic subjects and the Federal Government stringency index (GSI). The GSI [50] is a composite measure based on nine response indicators including school closures, workplace closures, and travel bans, rescaled to a value from 0 to 100 (100 = strictest). If policies vary at the level of federal states, the index is shown for the state with the strictest measures. For background info see also [51]. Colors of curves correspond to different y-axes.

While Saxony was almost spared from the first wave of SARS-CoV-2 in Germany, the second wave hit the country particularly hard resulting in the highest relative death toll of all German states (1 out of 400 inhabitants of Saxony died from COVID-19 during the second and the immediately following B.1.1.7-driven third wave). The second wave was on its peak in the middle of December 2020. A hard lock-down was initiated at this time including closure of schools, prohibition of all team-based leisure activities, and night-time curfew. We were asked by the government to estimate the length of lock-down required to break the second wave. Stringency of lock-down was comparable to the first wave. Thus, we simulated four scenarios: an optimistic assumption of a lock-down efficacy of 60% reduction in infectivity, a more realistic scenario with 40% reduction, a pessimistic assumption of only 20% lock-down efficacy, and finally, 0% reduction (no lock-down) as control scenario. Results are shown in Figure 6 and revealed a good agreement of our prediction with the actual course for the 40% scenario considered likely.

At the beginning of February 2021, the second wave was broken in Saxony and first relaxations of NPIs were conducted. At this time, the more virulent B.1.1.7 variant became endemic in Germany. At 14 February, the true percentage of the B.1.1.7 variant was unknown due to lack of sequencing capacities. Moreover, there were uncertainties with respect to the increase in infectivity by the B.1.1.7 variant. We therefore simulated three scenarios (optimistic: 10% initial proportion of B.1.1.7, infectivity increased by factor 1.7, expected: 20% initial proportion, 1.8-times increase in infectivity, pessimistic: 30% initial proportion, 2-times increase in infectivity). Results are shown in Figure 7. The actual course of the epidemic was close to the pessimistic scenario, i.e., the second wave was directly followed by a third wave due to the B.1.1.7 variant. Indeed, later data revealed that the proportion of B.1.1.7 was already close to 30% (pessimistic assumption) at the time the simulation was performed. Moreover, our model correctly predicted the variant replacement by B.1.1.7.

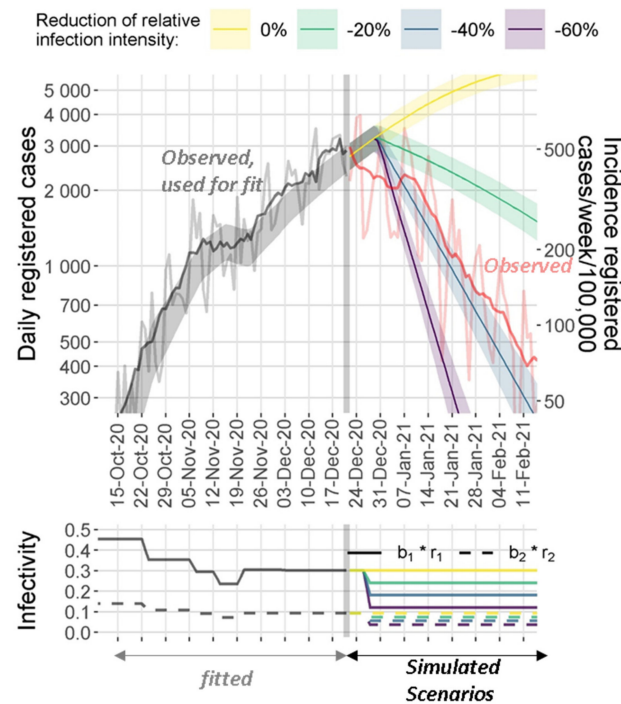


Figure 6. Comparison of predicted and observed decline of the second wave in Saxony according to the initiated lock-down. Our model was used to fit the observed data until 21 December 2020 (shown as grey curve (raw data) and black curve (smoothed) of reported test-positives). Estimated step functions b_1 and b_2 describing the infectivity of asymptomatic and symptomatic subjects were reduced by 0% (yellow: no lock-down = control scenario), 20% (green: pessimistic scenario), 40% (blue: realistic scenario), and 60% (magenta: optimistic scenario) to simulate four scenarios of the future course of the epidemic under lock-down conditions. The observed numbers of test-positives after the 21 December 2020 are shown in red (light red = raw data, dark red = smoothed) closely followed the expected scenario of 40% lock-down efficacy. Shaded areas represent 95% prediction intervals. The predictions and parameters were reported in our regular bulletin deposited at Leipzig Health Atlas, ID: 85AH9JMUFM-4.

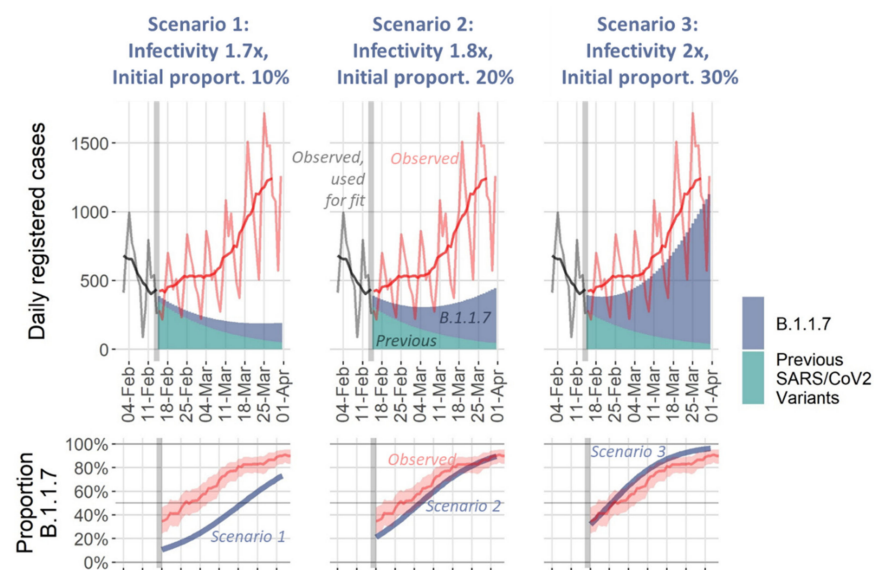


Figure 7. Simulation of third wave scenarios for Saxony/Germany: Upper row: The model was used to fit all observed data until 14 February 2021 (grey curve = raw data of reported testpositives,

black curve = smoothed). Three scenarios were simulated differing in assumed initial proportion of B.1.1.7 which was not exactly known at this time point (10%, 20%, and 30%, respectively) and in the assumptions regarding increased virulence of B.1.1.7 (parameter μ = 1.7, 1.8 and 2, respectively). Predicted course of subjects infected with the respective variants are shown as shaded areas. The observed total numbers of testpositives (light red = raw data of reported testpositives, dark red = smoothed curve) closely followed the pessimistic scenario 3. Lower row: When comparing the proportion of B.1.1.7 as retrieved from [52] from 18 July 2021, initial proportion of B.1.1.7 was indeed close to that assumed for scenario 3. Blue curves represent 95% confidence intervals of the B.1.1.7 proportion predicted for the different scenarios. All predictions were reported in our bulletin at the 20 February 2021 deposited at our Leipzig Health Atlas [53].

4. Discussion

In this paper, we propose a method of parametrization of COVID-19 epidemiologic models and applied it to an extended SECIR-type model to explain the course of the epidemic in Germany and one of its federal state, the Free State of Saxony. Moreover, we demonstrated how the model can be used to make relevant predictions, which could be validated on the basis of subsequent observational data.

A key idea of our approach is the embedding of differential equations-based epidemic modelling into an input-output dynamical system (IO-NLDS). This has two major advantages. First, the approach allows combining explicit mechanistic models of epidemic spread and phenomenological considerations of external impacts on model parameters via the input layer. This allows parametrizing models of different complexity. For example, in our model we non-explicitly considered the effect of age structures of the diseased population by time-dependent input parameters such as probabilities of critical disease courses and deaths. This could easily be replaced for example by age-structured models. We believe that such a combined empirical/mechanistic approach is well suitable to address the complexity of COVID-19 epidemic dynamics for which it is impossible to consider all relevant mechanisms explicitly and in parallel.

The second major advantage of our approach is that we assumed a non-direct link between state parameters of the embedded SECIR model and observables. This allows interposing a data model considering known biases of the available data resources. We aimed at identifying relevant bias sources as far as possible and considered them in our proposed data models. However, these data models could be subjected to changes in the future for example if better data of COVID-19-related death will be released. Improved data models could be easily integrated into our framework.

Note that the IO-NLDS implementation translates the embedded differential equations model to a discrete scale (i.e., days in our case), which however appears to be sufficient for describing an epidemic.

We also want to note that the SECIR model used here is by far neither unique nor the most comprehensive one. For example, The Robert-Koch institute developed a model for the purpose of estimating the effect of different vaccination strategies which could easily be included into our SECIR-type models [54]. Although integration of differential equations-based models into our IO-NLDS context is more straightforward, our approach is also applicable to agent-based models. In general, the aspect of parameter estimation of such models is underdeveloped in view of the highly biased data resources used and to our knowledge, no generic concept was proposed so far.

Based on our IO-NLDS formulation and data models, we parametrized our model on the basis of data of infection numbers, critical cases, and deaths available for Germany and Saxony. Here, we chose a full-information approach considering all data in between start of the epidemic 4 March 2020 to 29 March 2021. We also applied a Bayesian learning process by considering other studies to inform model parameter's settings. Thus, we combine mechanistic model assumptions with results from other studies and observational data. This approach is very popular in pharmacology [55] but despite its importance it is yet rarely applied in epidemiology [11]. It resulted in a complex likelihood function, which is

optimized on the basis of Markov-Chain Monte Carlo (MCMC) algorithms, as we described in Appendices B and F. If the likelihood has a unique maximum, most of the samples eventually accumulate in its vicinity after a certain number of “burn-in” steps. This allows an effective MCMC search of the best parameter estimates as well as approximations of their standard errors (standard deviations of the sample) and the degree of overfitting. However, if parameters are interdependent, MCMC algorithm samples manifolds of alternative solutions, resulting in large standard errors of the overfitted parameters. We successfully addressed this issue by a modified version of Maire’s algorithm [56]. Central to this approach is the idea that the proposal distribution adapts to the target by locally adding a mixture component when the discrepancy between the proposal mixture and the target is deemed to be too large. In other words, this algorithm samples multidimensional parameters sets, approximating it as a mixture of multivariate Gaussian distribution. Such approaches enable adequate sampling of model parameters and detection of overfitting as well as of multiple local maxima of the likelihood. Our results revealed small standard errors indicating lack of overfitting, see Tables A1 and A3 from Appendix I, Tables A6 and A7 from Appendix J. We also applied rigorous information criteria to limit the number of steps of our input functions. As a consequence, it was possible to identify both, the fixed parameters of the SECIR model and the time-variable input functions representing changing NPI/contact behavior and age-structures.

Model parametrization resulted in a good and unbiased fit of data for the period considered for Germany. Fixed parameter values of the SECIR model did not significantly deviated from their prior values if available. It required 18 respectively 19 steps of changes of the probabilities to develop critical stage and to die respectively. A total of 13 intensification and 15 relaxation events were necessary to describe the epidemic dynamics over the time course of observations. Estimated infectivity roughly correlated with the Governmental Stringency Index [51]. We regularly contributed forecasts of our model to the German forecast Hub [57].

We also demonstrated utility of our model by several mid-term simulations of scenarios of epidemic development in Saxony, a federal state of Germany. We could show that predictions of reported infections were in the range of later observations for scenarios considered likely.

As future extensions and improvements of our model, we will consider stochastic effects on a daily scale, for example to model random influxes of cases or to model random extinctions of infection chains. These effects are relevant to be considered in times of low incidence numbers such as those observed in Germany in the summers 2020 and 2021. Our IO-NLDS framework is well suited to implement such extensions [17].

In future versions of our model, we will also include age-structures and implement a vaccination and waning model in analogy to other research groups. In the current version of the model, we assumed a constant proportion of symptomatic patients reported as infected. This does not consider for example changing testing policies (i.e., symptomatic vs. prophylactic testing). We plan to refine our model in this regard in the future. Finally, we will consider the Delta and Omicron variants emerging in 2021 [53] in the next update of our SECIR model.

In summary, the primary focus of the paper is an adequate parametrization of epidemiological models on the basis of complex, possibly biased data, as well as its coupling with structurally unknown dynamical external influences. This approach allows for a clear separation of mechanistic model compartments from random or time-dependent non-mechanistic influences and biases in the data. We believe that this approach is useful not only for the parametrization of the SECIR model presented here but also for other epidemiologic models including other disease contexts and data structures.

Author Contributions: Conceptualization (ideas; formulation or evolution of overarching research goals and aims): H.K. and M.S.; data curation (management activities to annotate (produce metadata), scrub data and maintain research data (including software code, where it is necessary for interpreting the data itself) for initial use and later reuse): H.K.; formal analysis (application of statistical, mathematical, computational, or other formal techniques to analyze or synthesize study data): Y.K.; funding acquisition (acquisition of the financial support for the project leading to this publication): M.S.; investigation (conducting a research and investigation process, specifically performing the experiments, or data/evidence collection): Y.K., H.K. and M.S.; methodology (development or design of methodology; creation of models): Y.K., M.S. and H.K.; project administration (management and coordination responsibility for the research activity planning and execution): M.S.; resources (provision of study materials, reagents, materials, patients, laboratory samples, animals, instrumentation, computing resources, or other analysis tools): H.K.; software (programming, software development; designing computer programs; implementation of the computer code and supporting algorithms; testing of existing code components): Y.K. and H.K.; supervision (oversight and leadership responsibility for the research activity planning and execution, including mentorship external to the core team): M.S.; validation (verification, whether as a part of the activity or separate, of the overall replication/reproducibility of results/experiments and other research outputs): H.K. and M.S.; visualization (preparation, creation and/or presentation of the published work, specifically visualization/data presentation): H.K., writing—original draft preparation (creation and/or presentation of the published work, specifically writing the initial draft (including substantive translation)): Y.K., H.K. and M.S.; writing—review and editing (preparation, creation and/or presentation of the published work by those from the original research group, specifically critical review, commentary or revision—including pre- or post-publication stages): Y.K., H.K. and M.S. All authors have read and agreed to the published version of the manuscript.

Funding: This project was funded in the framework of the project SaxoCOV (Saxonian COVID-19 Research Consortium). SaxoCOV was financed by the Free State of Saxony. Presentation of data, model results and simulations were funded by the NFDI4Health Task Force COVID-19 (www.nfdi4health.de/task-force-covid-19-2, accessed on 20 June 2022) within the framework of a DFG-project (LO-342/17-1). Epidemiological modeling was also supported by the German Federal Ministry of Education and Research (BMBF) within the framework of the e:Med line of funding (CAPSyS, grant number 01ZX1304A) and the project PROGNOSIS (grant number #031L0296A).

Institutional Review Board Statement: Ethical review and approval were waived for this study as only published data from official sources was used (see manuscript for detailed description of data sources).

Informed Consent Statement: Patient consent was waived for this study as only published data from official sources was used (see manuscript for detailed description of data sources).

Data Availability Statement: Code and data are shared. <https://www.health-atlas.de/models/40> and GitHub <https://github.com/GenStatLeipzig/LeipzigMISE-SECIR>.

Conflicts of Interest: The authors declare no conflict of interest.

Appendix A. Equations of the SECIR Model

We here present the equations of the SECIR model serving as hidden layer of our input-output non-linear dynamical system (IO-NLDS). To fit in this context, the ordinary differential equations of the SECIR model are approximated by a difference equation system describing compartment changes at single days, i.e., time-steps Δt equals one day. Compartments of the model are explained in Table 1 of the main paper. Parameters are explained in Table 2 of the main paper.

$$\begin{aligned}
\frac{\Delta S_c}{\Delta t} &= -influx - Influx_E - Influx_E^{Mu} \\
\frac{\Delta E}{\Delta t} &= influx + Influx_E - r_3 \cdot E \\
\frac{\Delta I_{A,1}}{\Delta t} &= r_3 \cdot E - (X(r_{4,b}, r_4, p_{symp}) \cdot r_{4,b} + (1 - X(r_{4,b}, r_4, p_{symp})) \cdot r_4) \cdot I_{A,1} \\
\frac{\Delta I_{A,2}}{\Delta t} &= (1 - X(r_{4,b}, r_4, p_{symp})) \cdot r_4 \cdot I_{A,1} - r_4 \cdot I_{A,2} \\
\frac{\Delta I_{A,3}}{\Delta t} &= r_4 \cdot I_{A,2} - r_4 \cdot I_{A,3} \\
\frac{\Delta I_{S,1}}{\Delta t} &= X(r_{4,b}, r_{4,b}, p_{symp}) \cdot r_{4,b} \cdot I_{A,1} - (X(r_6, r_5, p_{crit}) \cdot r_6 + (1 - X(r_6, r_5, p_{crit})) \cdot r_5) \cdot I_{S,1} \\
\frac{\Delta I_{S,2}}{\Delta t} &= (1 - X(r_6, r_5, p_{crit})) \cdot r_5 \cdot I_{S,1} - r_5 \cdot (1 - p_{death,S}) \cdot I_{S,2} - p_{death,S} \cdot r_8 \cdot I_{S,2} \\
\frac{\Delta I_{S,3}}{\Delta t} &= (1 - p_{death,S}) \cdot r_5 \cdot I_{S,2} - r_5 \cdot I_{S,3} \\
\frac{\Delta C_1}{\Delta t} &= X(r_6, r_5, p_{crit}) \cdot r_6 \cdot (I_{S,1} + I_{S,1}^{Mu}) - (X(r_8, r_7, p_{death}) \cdot r_8 + (1 - X(r_8, r_7, p_{death})) \cdot r_7) \cdot C_1 \\
\frac{\Delta C_2}{\Delta t} &= (1 - X(r_8, r_7, p_{death})) \cdot r_7 \cdot C_1 - r_7 \cdot C_2 \\
\frac{\Delta C_3}{\Delta t} &= r_7 \cdot C_2 - r_7 \cdot C_3 \\
\frac{\Delta R}{\Delta t} &= r_5 \cdot (I_{S,3} + I_{S,3}^{Mu}) + r_7 \cdot C_3 + r_4 \cdot (I_{A,3} + I_{A,3}^{Mu}) \\
\frac{\Delta D}{\Delta t} &= X(r_8, r_7, p_{death}) \cdot r_8 \cdot C_1 + p_{death,S} \cdot r_8 \cdot (I_{S,2} + I_{S,2}^{Mu})
\end{aligned} \tag{A1}$$

With the abbreviations

$$\begin{aligned}
Influx_E &= r_1 \cdot b_1 \cdot Sc \cdot (I_{A,1} + I_{A,2} + I_{A,3}) + r_2 \cdot b_2 \cdot Sc \cdot (I_{S,1} + I_{S,2} + I_{S,3}) \\
Influx_E^{Mu} &= Mur \left(r_1 \cdot b_1 \cdot Sc \cdot (I_{A,1}^{Mu} + I_{A,2}^{Mu} + I_{A,3}^{Mu}) + r_2 \cdot b_2 \cdot Sc \cdot (I_{S,1}^{Mu} + I_{S,2}^{Mu} + I_{S,3}^{Mu}) \right)
\end{aligned}$$

At this, we assume that asymptomatic and symptomatic compartments have different time-dependent infectivity ($r_1 * b_1$, $r_2 * b_2$), with b_1 and b_2 later defined on the basis of time-dependent NPI/behavioral changes and, for parsimony, $b_1 = b_2$. Hence, the ratio of the products ($r_1 * b_1$) and ($r_2 * b_2$) is assumed constant. Factor of increased infectivity of new virus variant *mur*: this factor is multiplied to r_1 and r_2 reflecting higher infectivity of the B.1.1.7 variant compared to the previous variants. The superscript Mu denotes new virus variants.

The functions X represent decisions regarding the further disease course defined below.

Analogously, the equations for the concurrent variant compartments are as follows:

$$\begin{aligned}
 \frac{\Delta E^{Mu}}{\Delta t} &= Influx_E^{Mu} - r_3 \cdot E^{Mu} \\
 \frac{\Delta I_{A,1}^{Mu}}{\Delta t} &= r_3 \cdot E^{Mu} - (X(r_{4,b}, r_4, p_{symp}) \cdot r_{4,b} + (1 - X(r_{4,b}, r_4, p_{symp})) \cdot r_4) \cdot I_{A,1}^{Mu} \\
 \frac{\Delta I_{A,2}^{Mu}}{\Delta t} &= (1 - X(r_{4,b}, r_4, p_{symp})) \cdot r_4 \cdot I_{A,1}^{Mu} - r_4 \cdot I_{A,2}^{Mu} \\
 \frac{\Delta I_{A,3}^{Mu}}{\Delta t} &= r_4 \cdot I_{A,2}^{Mu} - r_4 \cdot I_{A,3}^{Mu} \\
 \frac{\Delta I_{S,1}^{Mu}}{\Delta t} &= X(r_{4,b}, r_{4,b}, p_{symp}) \cdot r_{4,b} \cdot I_{A,1}^{Mu} - (X(r_6, r_5, p_{crit}) \cdot r_6 + (1 - X(r_6, r_5, p_{crit})) \cdot r_5) \cdot I_{S,1}^{Mu} \\
 \frac{\Delta I_{S,2}^{Mu}}{\Delta t} &= (1 - X(r_6, r_5, p_{crit})) \cdot r_5 \cdot I_{S,1}^{Mu} - r_5 \cdot (1 - p_{death,S}) \cdot I_{S,2}^{Mu} - p_{death,S} \cdot r_8 \cdot I_{S,2}^{Mu} \\
 \frac{\Delta I_{S,3}^{Mu}}{\Delta t} &= (1 - p_{death,S}) \cdot r_5 \cdot I_{S,2}^{Mu} - r_5 \cdot I_{S,3}^{Mu}
 \end{aligned}
 \tag{A2}$$

In some of the compartments, there is a decision between recovery or deterioration of the disease course. For example, patients in C_1 can either die or recover with different rates r_i and r_j . To model this decision, we split the number of patients in the compartment by a respective probability p and determine the decision factor X as follows.

$$\frac{r_i X}{r_j (1 - X)} = \frac{p}{1 - p}$$

Thus

$$X(r_i, r_j, p) = \frac{r_j p}{r_i \cdot (1 - p) + r_j \cdot p}
 \tag{A3}$$

To start the epidemic in Germany, we assumed an entry of infected cases by a linearly decreasing function starting at 4 March 2020 and becoming zero at 10 March 2020. Occurrence of the B.1.1.7 variant was initialized by a single influx to $E^{Mu}, I_{A,1}^{Mu}, I_{A,2}^{Mu}, I_{A,3}^{Mu}, I_{S,1}^{Mu}, I_{S,2}^{Mu}, I_{S,3}^{Mu}$ at the 26 February 2021. We assume that the ratio between these influxes are the same as those for the normal variant compartments at this day. The sum of $E^{Mu}, I_{A,1}^{Mu}, I_{A,2}^{Mu}, I_{A,3}^{Mu}, I_{S,1}^{Mu}, I_{S,2}^{Mu}, I_{S,3}^{Mu}$ at 26 February 2021 was fitted to be 5.3% of the corresponding sum of the normal compartments at the same day.

Appendix B. Input Layer

The input layer of our IO-NLDS is designed to describe the effects of non-pharmaceutical interventions (NPI) and other impacts on infectivity such as behavioral changes, changes in age-structure, testing policy, seasonal effects, or larger outbreaks (abbreviated as NPI/contact behaviour). Since these effects typically affect contact matrices in different ways, we model this phenomenologically by time-dependent reductions or increases of infection rates caused by symptomatic and asymptomatic subjects as explained in Equation (A1).

We make the following assumptions for non-pharmaceutical interventions:

1. We introduce the relative infectivity function $b(t)$, which changes according to NPI/contact behavior modifications. This is modelled by a linear increase (in case of relaxation) or decrease (in case of tightening) within a fixed time Del_{tr} of two days. Otherwise, $b(t)$ is constant. We denote $\{T_{tr,s}\}_{s=1}^{N_{tr}}$ as the time points with changes in non-pharmaceutical interventions with N_{tr} the total number of time points with changes. We collected dates of changing non-pharmaceutical intervention measures for Germany based on government decisions, changing testing policies as well as events with impact on epidemiological dynamics such as holidays and sudden outbreaks (such as thin peak of new infections in June affected mostly workers of the meat industry). We also assumed additional time points with changes determined by BIC.

Again, for the sake of parsimony, we assume that the relative infection intensities of asymptomatic ($b_1(t)$) and symptomatic subjects ($b_2(t)$) are the same, hence, respective proportionality $rb_{1,2}$ is constant and estimated during model fitting.

Thus, $b(t)$ is defined as follows:

$$\begin{aligned}
 b(t) = \begin{cases} b_{tr,s-1}, & t \in [T_{tr,s-1} + Del_{tr}, T_{tr,s}] \\ \frac{b_{tr,s-1}}{Del_{tr}} \cdot (Del_{tr} - t + T_{tr,s}) + \frac{b_{tr,s}}{Del_{tr}} \cdot (t - T_{tr,s}), & t \in [T_{tr,s}, T_{tr,s} + Del_{tr}] \\ b_{tr,s}, & t \in [T_{tr,s} + Del_{tr}, T_{tr,s+1}] \end{cases} \tag{A4} \\
 b_{tr,0} = 1 \\
 b_1(t) = b(t) \\
 b_2(t) = b_1(t)
 \end{aligned}$$

The time point $t = 0$ corresponds to the 3 March 2020.

2. Likewise, rates toward critical disease states and deaths are also assumed to vary through the course of the epidemic due to changes in testing policy resulting in different percentages of unreported cases and asymptomatic subjects, changes in age distribution of infected subjects, improvement of patient care due to new treatment options and due to possible over-stretched medical resources (not the case in Germany but other countries). In our model, this is also accounted for phenomenologically by assuming the probabilities p_{crit} and p_{death} as time-dependent input parameters.

We assume that both functions are step functions:

$$p_{crit}(t) = p_{crit,0} \cdot \sum_{j=0}^{N_{crit}-1} \alpha_{crit,j} \cdot \chi_{[T_{pcrit,j}, T_{pcrit,j+1})}(t) \tag{A5}$$

where $\{T_{pcrit,j}\}_{j=1}^{N_{crit}}$ are empirical dates and $\{\alpha_{crit,j}\}_{j=1}^{N_{crit}}$ the respective relative changes of p_{crit} . Both, $\{T_{pcrit,j}\}_{j=1}^{N_{crit}}$ as well as $\{\alpha_{crit,j}\}_{j=1}^{N_{crit}}$ are parameters to be estimated. The initial value of p_{crit} is $p_{crit,0}$. Functions $\chi_{[t_j, t_{j+1})}(t)$ are indicator functions being 1 in the interval $[T_{pcrit,j}, T_{pcrit,j+1})$ and 0 else.

The step functions for $p_{death}(t)$ and $p_{death,S}(t)$ are defined analogously:

$$\begin{aligned}
 p_{death}(t) &= p_{death,0} \cdot \sum_{j=0}^{N_{death}-1} \alpha_{death,j} \cdot \chi_{[T_{pdeath,j}, T_{pdeath,j+1})}(t) \tag{A6} \\
 p_{death,S}(t) &= p_{death,S,0} \cdot p_{death}(t)
 \end{aligned}$$

The partitions of p_{crit} and p_{death} are assumed independent. Respective numbers of jumps N_{crit} and N_{death} can differ.

In order to find an optimal tradeoff between parsimony and goodness of fit we calculated Bayesian Information criteria (BIC) for different partition numbers N_{tr} , N_{crit} , and N_{death} and chose partitions minimizing BIC.

When new data become available, we attempt to update the numbers of partitions every two weeks by considering adding a new break-point within the last month. The time point as well as the corresponding jump value are considered as two new parameters. We added a new break point only if it improves BIC after the updated parameters estimation.

Appendix C. Output Layer

We here describe, how the state parameters of the hidden SECIR model are linked with data via the output layer of the IO-NLDS.

Modeling of daily registered infected cases $I_{S,M}$: The total number of daily registered infected cases $I_{S,M}$ is coupled to the efflux of the first asymptomatic compartments $I_{A,1}$ and $I_{A,1}^{Mu}$ toward symptomatic compartments multiplied with $P_{S,M}$.

$$I_{S,M}(T) = \sum_{t=0}^T P_{S,M} \cdot X(r_{4,b}, r_4, p_{symp}) \cdot r_{4,b} \cdot (I_{A,1}(t) + I_{A,1}^{Mu}(t)) \tag{A7}$$

However, we assume a delay of the registered vs. reported cases by introducing an empirical distribution of the reporting delay: When a person has a positive PCR SARS-CoV-2 test result at a date d_1 , this will result in a registered case at a later date d_2 . The difference $d = d_2 - d_1$ is the reporting delay and is assumed log-normally distributed. This distribution of delays is determined on the basis of data provided by the Robert-Koch-Institute from the period 27 April 2020 to 13 November 2020. The parameters of this distribution are derived by minimizing the Kullback–Leibler divergence between the parametric representation and the empirical distribution. Results are displayed in Figure A1.

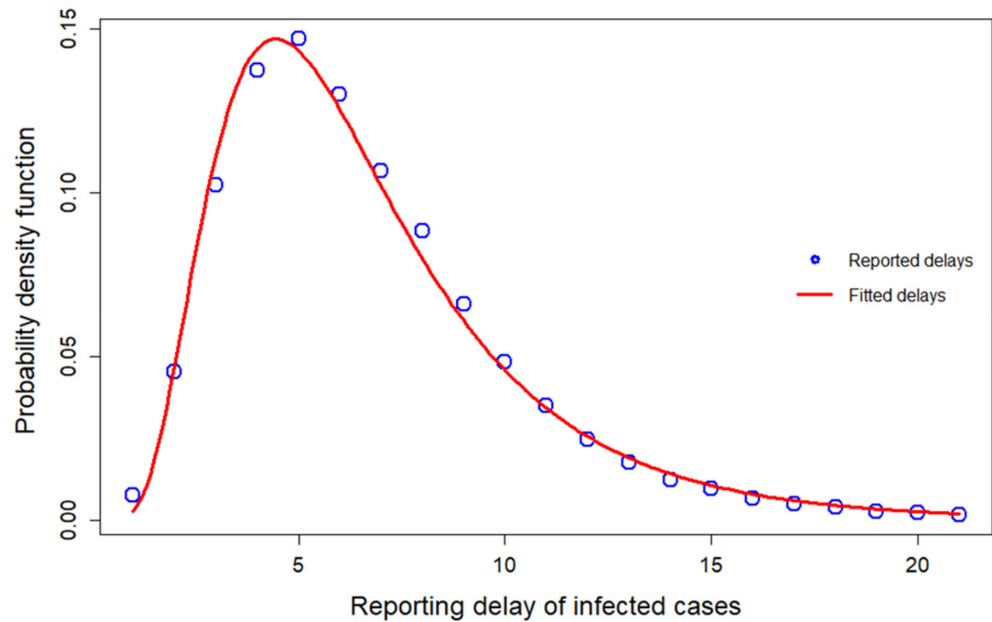


Figure A1. Approximation of reporting delay by a log-normal distribution: We present the log-normal distribution best fitting the empirical distribution of reporting delays. Estimated parameters of the log-normal distribution are as follows: $\mu = 1.77$ days, $\sigma = 0.531$ days.

Modeling delay of death reporting: In contrast to the newly infected cases, neither information of delays in COVID-19 associated death reporting nor actual dates of deaths were available to us. Therefore, we used a data model proposed by Delagdo et al. [45]. In detail, we assumed that the delay is normally distributed with an average of 7.14 days and a standard deviation of 4 days.

Since we consider time as an integer, we discretize this normal distribution by the approximation $DRD(d) = \frac{N_{7.14,4}(d)}{\sum_{i=1}^{100} N_{7.14,4}(i)}$ for integers $d \leq 100$ and 0 else, where N is the Gaussian distribution function with mean 7.14 days and standard deviation of 4 days, i.e., we neglect delays larger than 100 days. Using this approximation, we derive the actual number of new deaths at time point t :

$$D_a(t) = \sum_{t1 < t} Dr(t) \cdot DRD(t - t1)$$

Here, $Dr(t)$ is the number of reported new deaths at time t . The function $D_a(t)$ is linked to our compartment D .

Appendix D. Parameter Estimation

Free parameters of the model are determined by minimizing the negative log-likelihood function of observed data. The negative likelihood is constructed in analogy to [47]. It constitutes of the sum of three components:

$$nLL = nLL^{pri} + nLL^{resid} + Constr \quad (A8)$$

The terms nLL_i^{pri} and nLL_i^{resid} correspond to prior constraints of parameters and to the residual errors of the data as explained below in detail. The term *Constr* is a penalty term to keep values in eligible ranges or orders (see “Penalization”). We assume independence between parameters throughout.

Parameter distributions and transformations: Most of the parameters are confined to certain ranges. During estimation (with possible prior constraints), we transform these parameters to the space of real numbers. We assume that these transformed values are normally distributed during Markov-Chain Monte Carlo (MCMC) sampling (see below). To ensure this, parameters confined to a finite interval (a,b) are transformed by the *logit*-function. Parameters with positive values are transformed by a log-normal transformation. Thus,

$$\varphi_s = h_k(\psi_s)h_s(\psi_s) = \begin{cases} e^{\psi_s}, & \text{for parameters } > 0 \\ a + (b - a) \cdot \frac{e^{\psi_s}}{1 + e^{\psi_s}}, & \text{for parameters within } [a, b] \end{cases}, s = 1, \dots, N_{par} \quad (A9)$$

where φ_s is the s -th parameter and ψ_s is the respective transformed parameter and N_{par} is the total number of parameters to be estimated.

The negative likelihood contribution of the priors nll_i^{pri} is defined as follows:

$$nLL^{pri} = \sum_{s=1}^{N_{par}} \delta_s \cdot \frac{(\psi_s - \psi_s^{pri})^2}{\omega_{pri,s}^2} \quad (A10)$$

where δ_s equals 1, if a prior is assumed for the s -th parameter and 0 otherwise. The prior information is represented by the “best value” ψ_s^{pri} and an uncertainty expressed as standard deviation of possible values $\omega_{pri,s}$. We assume that parameter estimates are random variables normally distributed around their respective prior values. Thus,

$$\psi_s \sim N(\psi_s^{pri}, \omega_{pri,s}) = N\left(h_s(\varphi_s^{pri})^{-1}, \omega_{pri,s}\right) \quad (A11)$$

Prior “best values” and ranges of parameters are provided at Table 2 of the main paper. The uncertainties $\omega_{pri,k}$ are set to 2 for all parameters. This heuristic setting is based on a tradeoff between avoidance of overfitting including implausible parameter values and good data fitting properties.

Penalization: We penalize with a high value of 10^8 in cases when times of non-pharmaceutical interventions are either too close (closer than 3 days) or non-monotonic. In the same way, we penalize too high dynamical p_{death} values (more than 0.66) by multiplication of $\max(p_{death}-0.66, 0)$ with 100.

Residual errors of observed vs. predicted data: We fit data for daily registered cases, cumulative registered cases, deaths, cumulative deaths, and ICU occupation as explained in sub-section “output layer” and the methods section of the main paper. The respective term of the negative log-likelihood nll_i^{resid} corresponds to the residual errors of these data. Thus,

$$nLL^{resid} = \sum_{Y_{out}} \left(we_{dY_{out}} \cdot \sum_{j=1}^{N_{dY_{out}}} \frac{\left(dY_{out,S}^{tr_{dY_{out}}}(t_{j,dY_{out}}, \psi) - dY_{out,D}^{tr_{dY_{out}}}(t_{j,dY_{out}}) \right)^2}{a_{dY_{out}}^2} + we_{cumul} \cdot we_{Y_{out}} \cdot \sum_{j=1}^{N_{dY_{out}}} \frac{\left(Y_{out,S}^{tr_{Y_{out}}}(t_{j,dY_{out}}, \psi) - Y_{out,D}^{tr_{Y_{out}}}(t_{j,Y_{out}}) \right)^2}{a_{Y_{out}}^2} \right) \quad (A12)$$

where Y_{out} represents the output layers (“dY” corresponds to daily counts, while “Y” corresponds to cumulative counts). Subscript S denotes simulation results, while D corresponds to the data. We sum the negative log-likelihoods of the three outputs considered (infected subjects, critical cases and deaths). Thus, Y_{out} represents one of these three entities x with number of data points N_x at time points $\{t_{j,x}\}$ ($j = 1, \dots, N_x$) and residual errors a_x . We introduce weights we_{cumul} for the cumulative terms as compared with the daily counts and set it to 0.2. The cumulative terms were introduced to avoid biases of cumulative data occurring after fitting daily data only. Cumulative data for ICU occupation were not fitted, i.e., $we_{ICU} = 0$. The parameter $tr_{Y_{out}}$ corresponds to the power transformation used to compare model and data. In the present model version, it is set to 0.5. It constitutes a tradeoff between fitting precision of large and small numbers. All weights $we_{dY_{out}}$ and $we_{Y_{out}}$ were set to 1.

Thus, we assume that for each output and for each data point the entities $dY_{out,D}^{tr_{dY_{out}}}$ and $Y_{out,D}^{tr_{dY_{out}}}$ are normally distributed random variables around respective simulated values with standard deviations being the respective residual errors:

$$\begin{aligned} dY_{out,D}^{tr_{dY_{out}}}(t_{j,dY_{out}}) &\sim N\left(dY_{out,S}^{tr_{dY_{out}}}(t_{j,dY_{out}}, \psi), a_{dY_{out}}\right) \\ Y_{out,D}^{tr_{dY_{out}}}(t_{j,Y_{out}}) &\sim N\left(Y_{out,S}^{tr_{Y_{out}}}(t_{j,Y_{out}}, \psi), a_{Y_{out}}\right) \end{aligned} \quad (A13)$$

The algorithm to minimize the negative log-likelihood is explained in the next section. Differences of estimated values and their respective priors can be tested by calculating Z-scores $\frac{\psi_s - \psi_s^{pri}}{\omega_{pri,s}}$.

Appendix E. Algorithm for Parameter Estimations and Prediction Sampling

Due to nonlinearity of (Equations (A8), (A11) and (A12)), parameters ψ and residual errors θ cannot be estimated simultaneously. For such situations an expectation-maximization (EM) algorithm was proposed by Dempster et al. [58]. This algorithm is a widely applied approach for the iterative computation of maximum likelihood (correspondingly minimum of negative log-likelihood) estimates in incomplete-data statistical problems. In detail, the random parameters $\psi = \{\psi_s\}_{s=1}^{N_{par}}$ are considered as non-observed data, while observed data y in our case are defined as follows:

$$y = \left\{ \left\{ I_M^D(t_{j,IM}) \right\}_{j=1}^{N_{IM}}, \left\{ D^D(t_{j,D}) \right\}_{j=1}^{N_D}, \left\{ dI_M^D(t_{j,IM}) \right\}_{j=1}^{N_{dIM}}, \left\{ dD^D(t_{j,D}) \right\}_{j=1}^{N_{dD}}, \left\{ dICU_M^D(t_{j,ICU}) \right\}_{j=1}^{N_{dICU}} \right\} \quad (A14)$$

Complete data of the model is (y, ψ) . The unknown residual errors θ describe the uncertainty of parameters ψ .

Therefore $nLL(y, \psi; \theta)$ is a marginal negative log-likelihood likelihood. The complete likelihood nLL is defined as follows:

$$nLL(y; \theta) = \int_{\Omega} nLL(y, \psi; \theta) d\psi \quad (A15)$$

The EM algorithm minimizes $nLL(y; \theta)$ iteratively: At the k -th iteration of EM, the expectation step computes the conditional expectation of the complete negative log-likelihood $Q_k(\theta) = E(nLL(y, \psi; \theta) | y, \theta_{k-1})$ by generating $\psi^{(k)}$ based on previous estimates θ_{k-1} , and the maximization step computes the value θ_k maximizing $Q_k(\theta)$. The EM sequence (θ_k) converges to a stationary point under general regularity conditions [58].

In nonlinear cases, the expectation step cannot be performed in a closed form. Therefore, we applied the Stochastic Approximation algorithm of EM (SAEM). SAEM is a maximum likelihood estimator of the population parameters [48] based on stochastic integration of marginal probabilities without likelihood approximation such as linearization or quadrature approximation or sigma-point filtering [17]. Our implementation is inspired by and is very similar to that of earlier versions of Monolix (Lixoft) software (<http://lixoft.com/>, accessed on 16 November 2018)

The stochastic approximation version of standard EM algorithm (SAEM) proposed by [48] replaces the usual E-step at an iteration k by a stochastic procedure as follows:

1. Simulation step: draw m_k realizations of $\psi^{(k)} = \{\psi_s^{(k)}\}_{s=1}^{N_{par}}$ from the conditional distribution $p(\cdot | y; \theta_k)$ using MCMC algorithm.
2. Stochastic approximation: update $Q_k(\theta)$

$$Q_k(\theta) = Q_{k-1}(\theta) + \gamma_k \cdot \left(\frac{1}{m_k} \sum_{j=1}^{m_k} \log(p(y, \psi^{(k)}; \theta)) - Q_{k-1}(\theta) \right), \quad (A16)$$

where γ_k is a decreasing sequence of positive numbers.

3. Maximization-step (correspondingly, minimization for negative log-likelihood): update θ_k according to

$$\theta_{k+1} = \text{Arg min}_{\theta} (Q_k(\theta)) \quad (A17)$$

Remarks:

1. Our stochastic approximation step is an improved version of the stochastic approximation of the integration of marginal distribution on the multidimensional domain Ω of possible parameter values:

$$Q_k(\theta) = E(\log(p(y, \psi; \theta)) | y, \theta_{k-1}) = \int_{\Omega} \log(p(y, \psi^{(k)}; \theta_{k-1})) d\psi^{(k)} \quad (A18)$$

2. In analogy to Monolix software, we selected γ_k as follows:

$$\gamma_k = 1, \quad k \leq K_1$$

$$\gamma_k = \frac{1}{k - K_1 + 1}, \quad k > K_1 \quad (A19)$$

We choose K_1 equal to 4 and run the algorithm until convergence with a tolerance 0.1% of estimates of population parameters (see below).

3. We performed MCMC sampling 4000 times at each stage with a burn-in phase of 1000 steps. Thus, $m_k = 3000$.

Exact estimates of different components of θ_k are:

$$a_{dIM}^{(k)} = \sqrt{\frac{1}{N_{dIM}} \sum_{j=1}^{N_{dIM}} \int_{\Omega} (dI_M^S(t_{j,IM}, \psi^{(k)}) - dI_M^D(t_{j,IM}))^2 d\psi^{(k)}}$$

$$a_{dD}^{(k)} = \sqrt{\frac{1}{N_{dD}} \sum_{j=1}^{N_{dD}} \int_{\Omega} (dD^S(t_{j,D}, \psi^{(k)}) - dD^D(t_{j,D}))^2 d\psi^{(k)}} \quad (A20)$$

$$a_{dICU}^{(k)} = \sqrt{\frac{1}{N_{dICU}} \sum_{j=1}^{N_{dICU}} \int_{\Omega} (dICU^S(t_{j,ICU}, \psi^{(k)}) - dICU^D(t_{j,ICU}))^2 d\psi^{(k)}}$$

Therefore, respective stochastic approximations and maximizations θ_k are as follows:

$$s_{1,j,k} = s_{1,j,k-1} + \gamma_k \cdot \left(\frac{1}{m_k} \sum_{r=1}^{m_k} \left(dI_M^S(t_{j,IM}, \psi^{(k,r)}) - dI_M^D(t_{j,IM}) \right)^2 - s_{1,j,k-1} \right), j = 1, \dots, N_{dIM}$$

$$a_{dIM}^{(k)} = \sqrt{\frac{\sum_{j=1}^{N_{dIM}} s_{1,i,j,k}}{N_{dIM}}}$$
(A21)

$$s_{2,j,k} = s_{2,j,k-1} + \gamma_k \cdot \left(\frac{1}{m_k} \sum_{r=1}^{m_k} \left(dD^S(t_{j,IM}, \psi^{(k,r)}) - dD^D(t_{j,IM}) \right)^2 - s_{2,j,k-1} \right), j = 1, \dots, N_{dD}$$

$$a_{dD}^{(k)} = \sqrt{\frac{\sum_{j=1}^{N_{dD}} s_{2,i,j,k}}{N_{dD}}}$$
(A22)

$$s_{3,j,k} = s_{3,j,k-1} + \gamma_k \cdot \left(\frac{1}{m_k} \sum_{r=1}^{m_k} \left(dICU^S(t_{j,IM}, \psi^{(k,r)}) - dICU^D(t_{j,IM}) \right)^2 - s_{3,j,k-1} \right), j = 1, \dots, N_{dICU}$$

$$a_{dICU}^{(k)} = \sqrt{\frac{\sum_{j=1}^{N_{dICU}} s_{3,i,j,k}}{N_{dICU}}}$$
(A23)

In the same way, the respective terms for the cumulative data approximations are derived.

Appendix F. MCMC Algorithm for the Expectation Step

Markov chain Monte Carlo (MCMC) methods comprise a class of algorithms for sampling from a probability distribution [59]. By constructing a Markov chain that has the desired distribution as its equilibrium distribution, one can obtain a sample of the desired distribution by recording states from the chain. It is well-known that a proper choice of a proposal distribution for MCMC methods is a crucial factor for convergence of the algorithm [60]. For the sake of increasing the acceptance rate, a number of adaptive Metropolis (AM) algorithms were proposed by different groups. Here the proposal distribution is learned along the process using the full information cumulated so far. We implemented the adaptive MCMC version with Gaussian proposal distribution described in [60] as well as adaptive incremental Mixture MCMC [56] called AIMM, which we modified slightly. Strictly speaking, these methods are not really Markov chains, because proposal distribution of the next step depends on all preceding states $\left\{ \vec{X}_t \right\}_0^t$ rather than only the previous one. The algorithm of Haario et al. is simpler and it assumes the existence of a global minimum of nLL. In contrast, the algorithm of Maire et al. could be useful for cases when the nLL has a complex topology due to overfitting.

Let π denote the target distribution (i.e., negative log-likelihood) given by Equation (A8). At each iteration step the new parameter vector Y is generated by a transition kernel representing the proposal distribution. This candidate vector is accepted with probability

$$\alpha \left(\vec{X}_{t-1}, Y \right) = \min \left(1, \frac{\pi(Y)}{\pi \left(\vec{X}_{t-1} \right)} \right)$$
(A24)

The transition kernel of Haario’s MCMC version is an empirical covariance matrix of previous samples stabilized by an identity matrix multiplied by a small number ε :

$$C_t^{(k)} = s_d \cdot \left(cov \left(\psi^{(k,1)}, \dots, \psi^{(k,t-1)} \right) + \varepsilon \cdot Id \right), t \leq m_k,$$
(A25)

where t is a sampling number and $s_d = \frac{2.4}{\sqrt{N_{par}^{ind}}}$. Here, we choose $\varepsilon = 0.0001$. This parameter is required to ensure ergodic property of the Markov chain. When $k > 1$, we added samples from the previous step to the covariance matrix:

$$C_t^{(k)} = s_d \cdot \left(cov\left(\psi^{(k-1,1)}, \dots, \psi^{(k-1,m_k)}, \psi^{(k,1)}, \dots, \psi^{(k,t-1)}\right) + \varepsilon \cdot Id \right), t \leq m_k \quad (A26)$$

At each iteration k we used a sample from the previous iteration providing a small value of nLL as starting point.

In the AIMM, the proposal distributions Q_t are mixtures of multivariate normal distributions. Roughly spoken, this is a generalization of Haario's algorithm when multiple local minima of the nLL exist in few clusters. The candidate vector is accepted with probability

$$\alpha\left(\vec{X}_{t-1}, Y\right) = \min\left(1, \frac{\frac{\pi(Y)}{Q_t}}{\frac{\pi(\vec{X}_{t-1})}{Q_{t-1}}}\right) \quad (A27)$$

This algorithm minimizes discrepancies between proposal and target probability i.e., a sequence $\{Q_t\}$ converges to π by approximating it through mixtures of multivariate normal distributions. The elements of this series Q_t are defined as follows:

$$Q_t = \frac{\sum_{l=1}^{M_t} \beta_l \cdot \varphi_l}{\sum_{l=1}^{M_t} \beta_l},$$

where M_t is the number of components at the iteration t . The elements $\{\varphi_1, \dots, \varphi_{M_t}\}$ represent the incremental mixture components, $\{\beta_1, \dots, \beta_{M_t}\}$ are the respective weights. Each mixture component consists of a mean vector and a covariance matrix. The sampling from Q_t proceeds as follows: We choose the r -th component with a probability $\frac{\beta_r}{\sum_{l=1}^{M_t} \beta_l}$ by generating a uniformly distributed random number and accepting the r -th component if this number is in between $\left(\frac{\beta_{r-1}}{\sum_{l=1}^{M_t} \beta_l}, \frac{\beta_r}{\sum_{l=1}^{M_t} \beta_l}\right]$ if $r > 1$ or in between $\left[0, \frac{\beta_r}{\sum_{l=1}^{M_t} \beta_l}\right]$ if $r = 1$. After the choice of the r -th component, a random parameter vector Y is generated around the r -th mean according to the r -th covariance matrix as in Haario's algorithm. If Y is accepted, it becomes \vec{X}_t . \vec{X}_t can either stay in the r -th cluster or give origin for the new cluster φ_{M_t} with $M_t = 1 + M_{t-1}$. A new cluster is created when the match of φ_{M_t} to the r -th cluster is insufficient based on Mahalanobis distance. If \vec{X}_t stays in the r -th cluster, it updates the r -th covariance matrix in a similar way as in Haario's algorithm [60], Equation (A26).

We here modified the conditions for new cluster formation compared to [56] as follows. In our algorithm, a new cluster is formed when one of the following conditions hold:

- The Mahalanobis distance of \vec{X}_t to the cluster from which it was generated is less than 0.025 or larger than 0.975. That is \vec{X}_t diverges significantly from the current multivariate normal distribution of the r -th cluster
- $\pi(\vec{X}_t)$ is significantly larger than π of the current cluster center. That is \vec{X}_t does not correspond to the local maximum of π in the neighbourhood of the r -th cluster.

If one of the above conditions holds, \vec{X}_t becomes the center of a new cluster. The respective Gaussian component is the covariance matrix of the r -th (i.e., previous) cluster.

This matrix will be further updated every time when new members of the new cluster are accepted in future proposals.

The weights $\{\beta_1, \dots, \beta_{M_t}\}$ are proportional to π of the respective cluster centers to the power of γ , where γ is a positive number less than 1. All weights are updated every time when a new cluster emerges.

In summary, AIMM accepts proposals with discrepancies to the target distribution. As a consequence, proposal distributions are multivariate normal mixtures. Every cluster's mean is a local maximum of π . Sampling of proposal distributions from clusters depends on π . New clusters emerge when an accepted proposal either significantly diverges from the respective cluster's probability or when a significantly better optimal value is found in this cluster.

After thorough comparison of adaptive MCMC and the adaptive incremental mixture MCMC, we found the latter to be superior. Higher values of π were found in a shorter time. It also generates higher acceptance rates (0.2–0.3 versus 0.1) and finds more alternative solutions. We therefore used this method for our parameter estimations.

We applied Geweke convergence diagnostics for Markov chains [61] as implemented in the R-package *coda* (<https://cran.r-project.org/web/packages/coda/coda.pdf>, accessed on 01 October 2020). This method is based on a test for equality of the means of the first and last part of a Markov chain (by default the first 10% and the last 50%). If the samples are drawn from a stationary distribution of the chain, the two means are equal and Geweke's statistic has an asymptotical standard normal distribution. The test statistic is a standard Z-score: the difference between the two sample means divided by its estimated standard error. The standard error is estimated from the spectral density at zero taking autocorrelation into account. The Z-score is calculated under the assumption that the two parts of the chain are asymptotically independent. We applied this diagnostic for the nLL resulting from the last run of the implemented adaptive MCMC algorithm, resulting in a chain of 2620 steps. We considered default fractions of the chain, i.e., 0.1 and 0.5 of the beginning and from end of chain, respectively. The resulting Z-score is -0.2536 , corresponding to p -value of 0.4, i.e., no deviations of means were detected suggesting that a stationary distribution is achieved.

Figure A2 (generated by function `geweke.plot` from the *coda* package) shows the development of Geweke's Z-score when successively larger numbers of iterations are discarded from the beginning of the chain. The Z-score remains always in the 95% confidence interval, suggesting a successful convergence.

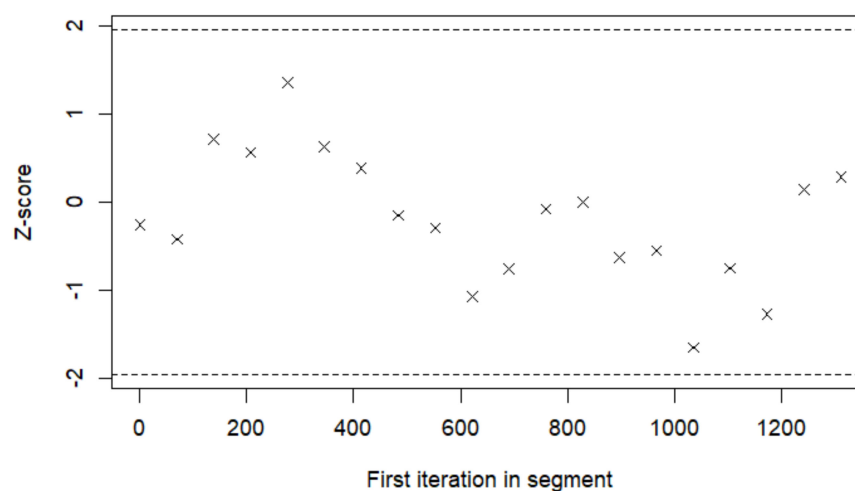


Figure A2. Development of Geweke's Z-score when successively larger numbers of iterations are discarded from the beginning of the MCMC chain. Dashed lines corresponds to quantiles of 0.025 and 0.095 for the Z-score. No local trends are detected, i.e., a stationary sampling distribution is achieved.

Appendix G. MCMC Simulation for Prediction and Controlling Goodness of Fit

The estimates of residual errors are determined at the last step and are used for MCMC sampling of parameters ψ . The resulting means and standard deviations are considered as respective average estimates and their standard errors. Simulations of these parameter samples provides a set of alternative predictions. From these, we collected the best fitting solution, the average solution and confidence intervals for different confidence limits α .

Appendix H. Justification of Prior Parameters and Ranges

We here provide justifications of assumed prior values and parameter ranges. Details of parameters definition and fitting can be found in Appendices B and D, respectively.

Initial influx of people per day *Influx*: The initial influx was estimated from the data without prior assumptions to a value of 6937 people per day in order to initialize the simulation. Later, the parameter is no longer relevant for simulation outcomes.

Infection rate through asymptomatic subjects per day r_1 : This infection rate was estimated from the data without prior assumptions. It represents the basic transmission probability of the SARS-CoV-2 virus from an asymptomatic infectious person to a susceptible contact.

Infection rate through symptomatic subjects per day r_2 : This infection rate was estimated from the data without prior assumptions. It represents the basic transmission probability of the SARS-CoV-2 virus from a symptomatic infectious person to a susceptible contact.

Relative infection intensity of asymptomatic subjects per day $b_1(t)$: The infectivity of asymptomatic infected subjects was assumed as a time-dependent step-function due to changing NPIs/contact behavior and other factors influencing infection probabilities. Steps were estimated from the data without prior assumptions.

Relative infection intensity of symptomatic subjects per day $b_2(t)$: The infectivity of symptomatic infected subjects was assumed as a time-dependent step-function due to changing NPIs/contact behavior and other factors influencing infection probabilities. Steps were estimated from the data without prior assumptions.

Ratio of $b_1(t)$ and $b_2(t)$ ($rb_{1,2}$). We assumed a fixed ratio of the infectivities of asymptomatic and symptomatic infected subjects for the sake of parsimony. The ratio was estimated from the data without prior assumptions.

Fixed dates for updates of infectivity functions: We used several fixed dates of changes in infectivity functions due to known changes in NPIs, testing policy or outbreaks. Note that even fixed time points were checked for necessity to assume changes in infectivity for the sake of parsimony, i.e., respective steps were only assumed if significantly improving model fit. The first three fixed time-points, tr_1 (10 March 2020), tr_2 (15 March 2020), and tr_3 (22 March 2020) reflect German governmental interventions including regulation of the size of public events, travel restrictions, and contact restriction. Fixed time-points tr_6 (30 April 2020), tr_7 (7 May 2020), and tr_8 (21 May 2020) reflect German governmental interventions related to the step-wise relaxation of NPIs, in particular regarding leisure sports, contacts, and schools. Time point tr_{17} (2 November 2020) reflects governmental NPIs in response to the German second wave, including restrictions of public life and social contacts, also referred as “soft lockdown”. Time point tr_{21} (16 December 2020) reflects further stricter governmental NPIs in response to the ongoing increase of the German second wave, also referred as “hard lockdown”, strongly limiting public and private contacts including school closures. Finally, time point tr_{28} (23 February 2021) reflects release of many governmental NPIs in response to the decline of the German second wave.

Transit rate for compartment E (latent time) r_3 : The transition rate r_3 for the compartment of exposed subjects is the inverse of the latent time, i.e., the time being infected but not yet infectious. The mean of the prior distribution for the latent time was set to 3 days and the minimum and maximum of the distribution was set to 2 and 4 days, respectively, in accordance with previous reports [10]. Note that minimum and maximum of a parameter’s distribution in this section always refer to the distribution of the mean of the parameter,

not of the distribution of the parameter itself. Further justification of this parameter is discussed in the following when considering the rate r_{4b} .

Transit rate for asymptomatic sub-compartments r_4 : The transition rate r_4 for the asymptomatic infectious compartment to the recovered compartment is a third of the inverse of the time being asymptomatic and infectious, as this compartment is split into three sub-compartments. The mean of the prior distribution of r_4 was set to 3/5 per day and the minimum and maximum of the distribution was set to 3/10 and 3/4 per day, respectively. These values are based on general considerations regarding timelines of the germinal center reaction [25] and further supported by reports from the literature estimating relevant infectiousness periods in general or asymptomatic/mildly symptomatic COVID-19 patients as in between 3.5 and 9.5 days [22–24].

Rate of development of symptoms after infection r_{4b} : The inverse of this rate is equal to the time from being infectious to start of developing symptoms. The mean of the prior distribution of r_{4b} was set to $\frac{1}{2}$.5 per day and the minimum and maximum of the distribution was set to 1/5 and 1/1 per day, respectively. This is in line with previous reports [10,26,27]. Note that the serial interval, i.e., the average time between successive cases in a chain of transmission is composed of two parameters of our model. In detail, the serial interval is the sum of the average latent time ($1/r_3$) and half of the average time being infectious when assuming random occurrence of subsequent infections during time of infectiousness. Exemplarily, if the serial interval would be considered in a scenario where symptomatic individuals are immediately and effectively quarantined, the serial interval would be $1/r_3 + 0.5 \cdot 1/r_{4b}$. The serial interval was estimated by the RKI [28] to have a median of 4 days (interquartile range 3–5 days) based on the literature [18–21], which is in accordance with our choices for r_3 and r_{4b} . However, the serial interval (and other parameters like the time being infectious) are to some extent also time dependent, reflecting e.g., behavioral changes. Although we do not model a time dependence for these specific parameters, our model can, to a certain extent, cope for this by data-driven adaptation of other time-dependent parameters such as b_1 and b_2 .

Probability of developing symptomatic disease after infection p_{symp} : This probability was estimated from the literature, reporting a percentage of symptomatic COVID-19 cases in between 55% and 85% [37–39]. We used a percentage of 50% as mean of the prior distribution, accounting for the fact that minor symptoms are frequently ignored or considered as symptoms of a common cold. Minimum and maximum was set to 0.3 and 0.8, respectively.

Transit rate of symptomatic sub-compartments r_5 : The transition rate r_5 for the three symptomatic sub-compartments towards recovery is a third of the inverse of time being symptomatic and infectious. The mean of the prior distribution of r_5 was set to 3/2.5 per day and the minimum and maximum of the distribution was set to 3/7.5 and 3/1.5 per day, respectively. These values are based on the assumption that symptomatic and asymptomatic subjects are similar with respect to time of contagiousness. Hence, values of the distribution of r_5 equal that of r_4 subtracted by the mean value of r_{4b} .

Rate of development of critical state after becoming symptomatic r_6 : The inverse of this rate is assumed equal to the time of developing a critical state after being infectious and symptomatic. The mean of the prior distribution of r_6 was set to 1/5 per day and the minimum and maximum of the distribution was set to 1/7 and 1/4 per day, respectively, according to previous reports [10,29–31]. Note that the probability of people becoming critical is affected by the function p_{crit} .

Probability of becoming critical after developing symptoms p_{crit} : This probability is assumed as a time-dependent step-function reflecting for example changing age-distributions of infected subjects or treatment efficacy. Steps were estimated from the data within the range of 0 to 1 without assuming a specific prior. The initial value of $p_{crit,0}$ was estimated as 0.075, which is within the range of reported values [10,62].

Transit rate for critical state sub-compartments r_7 : The transition rate r_7 for the critical state sub-compartments is a third of the inverse of the time treated in intensive care unit (ICU) for survivors, as the critical compartment is also split into three sub-compartments.

The mean of the prior distribution of r_7 was set to 3/17 per day and the minimum and maximum of the distribution was set to 3/35 and 3/8 per day, respectively. These values are informed by previous reports focusing on data of 35 to 79-year-old patients, the most frequent population in ICU [10,32–34].

Death rate of patients in critical sub-compartment r_8 : This transition rate represents the rate from the first ICU sub-compartment to the death compartment. It is the inverse of the time of patients in ICU that passed away. The mean of the prior distribution of r_8 was set to 1/8 per day and the minimum and maximum of the distribution was set to 1/14 and 1/6.5 per day, respectively. This reflects the shorter time in ICU for patients with fatal disease outcome informed by previous reports [29,35,36]. The number of people with fatal disease course is affected by two additional parameters p_{death} and $p_{death,S}$ explained below.

Probability of death after becoming critical p_{death} : This is the probability of death for patients at ICU. It is assumed as a time-dependent step-function estimated from data. Values are restricted within the range 0 to 1 without specific prior assumptions. Changes in time reflect for example changes in age-composition of ICU patients as well as changes in treatment regimens. The initial value is $p_{death,0} = 0.118$.

Probability of death after developing symptoms without becoming critical $p_{death,S}$: To reflect COVID-19 related deaths outside of ICU (especially relevant for the oldest age-groups [32]), we introduced the probability $p_{death,S}$ of transitioning from the second symptomatic sub-compartment to the death compartment. This probability was estimated from the data $p_{death,S} = 0.0448$.

Fraction of unreported cases $p_{S,M}$: For the fraction of infected cases that are symptomatic but not reported, we used a prior distribution with a mean of 0.5, a minimum of 0.3 and a maximum of 0.9. This choice was informed by studies of SARS-CoV-2 seroprevalence in Germany [40,41]. Note that the total percentage of unreported infected people is $1 - p_{S,M} \cdot p_{symp}$ according to the definition of p_{symp} .

The factor mur is multiplied to r_1 and r_2 reflecting higher infectivity of the B.1.1.7 variant compared to the previous variants. This parameter was estimated from sequencing data reporting the dynamics of the increase of variant B.1.1.7 in the UK, Denmark, Belgium, Suisse, and the United States, available from https://github.com/tomwenseleers/newcovid_belgium/, accessed on 13 April 2022) and Germany, available from “Mutationstracking-Projekt von Sven Schmidt” at <https://tinyurl.com/36xnmxat>, accessed on 17 May 2022). Thereby, mur was calibrated to match the observed average dynamic of the increase of B.1.1.7 across countries resulting in a value of $mur = 1.7$.

Appendix I. Parameter Values for Germany

Table A1. Time points of changes in infectivity and respective steps. We used fixed (known due to Governmental decisions or random events) and estimated time points of NPI/contact behavior changes and events and respective changes in infectivity of asymptomatic subjects. We provide estimates and relative standard errors of the infectivity. For estimated time points, we also provide the respective standard error (last column).

Number	Type of NPI/Contact Behaviour Change	Estimated New Infectivity	Relative Standard Error, %	Date	Source of Time Point	Standard Error (Days)
1	Intensification	0.676	0.738	10 March 2020	Fixed	-
2	Intensification	0.150	3.99	15 March 2020	Fixed	-
3	Relaxation	0.214	0.711	22 March 2020	Fixed	-

Table A1. Cont.

Number	Type of NPI/Contact Behaviour Change	Estimated New Infectivity	Relative Standard Error, %	Date	Source of Time Point	Standard Error (Days)
4	Intensification	0.131	2.79	29 March 2020	Estimated	0.280
5	Relaxation	0.172	2.78	23 April 2020	Estimated	0.164
6	Relaxation	0.200	0.462	30 April 2020	Fixed	-
7	Intensification	0.109	5.78	7 May 2020	Fixed	-
8	Relaxation	0.177	5.13	14 May 2020	Fixed	-
9	Intensification	0.163	0.278	22 May 2020	Estimated	0.322
10	Relaxation	0.434	0.644	5 June 2020	Estimated	0.387
11	Intensification	0.142	3.67	13 June 2020	Estimated	0.360
12	Relaxation	0.270	2.80	1 July 2020	Estimated	0.251
13	Intensification	0.193	1.06	11 August 2020	Estimated	0.244
14	Relaxation	0.256	1.01	28 August 2020	Estimated	0.264
15	Relaxation	0.357	1.06	1 October 2020	Estimated	0.119
16	Intensification	0.246	0.967	19 October 2020	Estimated	0.334
17	Intensification	0.198	3.98	2 November 2020	Fixed	-
18	Relaxation	0.213	0.991	11 November 2020	Estimated	1.08
19	Relaxation	0.256	0.550	24 November 2020	Estimated	0.262
20	Intensification	0.248	1.61	1 December 2020	Estimated	0.303
21	Intensification	0.118	2.18	16 December 2020	Fixed	-
22	Relaxation	0.421	1.40	26 December 2020	Estimated	0.238
23	Intensification	0.154	3.48	1 January 2021	Estimated	0.118
24	Relaxation	0.182	11.0	12 January 2021	Estimated	-
25	Relaxation	0.237	3.09	6 February 2021	Estimated	-
26	Intensification	0.211	4.08	15 February 2021	Estimated	-
27	Relaxation	0.233	2.98	25 February 2021	Estimated	-
28	Relaxation	0.228	23.2	18 March 2021	Fixed	-

Table A2. Determination of the number of time steps of input step functions. We analyzed different numbers of steps for the step functions p_{crit} (N_{crit}) and p_{death} (N_{death}). N_{par} = number of parameters to be estimated, nLL = negative log-likelihood, BIC = Bayesian information criterion. A total of 1714 data points were analyzed (348 new cases and death cases measurements daily and cumulative, 322 measurements of daily critical cases). The combination $N_{crit} = 18$ and $N_{death} = 19$ resulted in the lowest BIC , i.e., best compromise between model parsimony and fit. The best solution resulted from estimation of 134 parameters as follows: 15 basic parameters (Table A5), 28 of infectivity changes at 19 time points (Table A1), 18 values for $\alpha_{crit,i}$ with respect to 17 time points and 19 values for $\alpha_{death,i}$ with respect to 18 time points. Alternative assumptions on N_{crit} and N_{death} resulted in respective changes of the total number of parameters. The best results are in bold.

N_{crit}	N_{death}	N_{par}	nLL	BIC
18	19	134	2620	6238
17	17	132	2661	6298
17	19	133	2645	6280
18	18	133	2633	6256
19	20	136	2616	6245
19	19	135	2618	6241

Table A3. Step functions of p_{crit} and p_{death} . We present estimates for the single steps of the functions p_{crit} and p_{death} at the specified dates and respective standard errors. We also provide the standard error of the estimated time point (last column).

Parameter	Description	Estimate	Relative Standard Error. %	Date Respective Controls	Standard Error (Days)
$\alpha_{crit,1}$	Relative values of p_{crit} starting at the respective date	1.05	0.317	20 March 2020	0.0844
$\alpha_{crit,2}$		2.48	3.18	1 April 2020	0.14
$\alpha_{crit,3}$		2.24	3.46	6 May 2020	1.06
$\alpha_{crit,4}$		1.22	3.20	4 June 2020	2.03
$\alpha_{crit,5}$		0.884	0.626	6 July 2020	3.75
$\alpha_{crit,6}$		0.344	2.07	30 July 2020	1.14
$\alpha_{crit,7}$		0.340	0.381	24 August 2020	6.94
$\alpha_{crit,8}$		0.301	4.25	20 September 2020	0.705
$\alpha_{crit,9}$		0.238	1.15	6 October 2020	1.52
$\alpha_{crit,10}$		0.330	1.03	23 October 2020	1.42
$\alpha_{crit,11}$		0.382	0.801	8 November 2020	0.870
$\alpha_{crit,12}$		0.419	1.70	20 November 2020	6.20
$\alpha_{crit,13}$		0.633	1.53	23 December 2020	1.43
$\alpha_{crit,14}$		0.651	1.51	1 January 2021	0.506
$\alpha_{crit,15}$		0.929	1.12	22 January 2021	3.43
$\alpha_{crit,16}$		0.647	3.41	13 February 2021	3.08
$\alpha_{crit,17}$		0.394	0.972	5 March 2021	6.15
$\alpha_{crit,18}$		0.441	62.8	18 March 2021	-

Table A3. Cont.

Parameter	Description	Estimate	Relative Standard Error. %	Date Respective Controls	Standard Error (Days)
$\alpha_{death,1}$	Relative values of p_{death} starting at the respective date	2.39	1.88	26 March 2020	0.164
$\alpha_{death,2}$		3.58	1.17	23 April 2020	0.283
$\alpha_{death,3}$		1.94	4.55	19 May 2020	1.45
$\alpha_{death,4}$		0.743	1.19	10 June 2020	0.393
$\alpha_{death,5}$		0.296	3.25	5 July 2020	5.72
$\alpha_{death,6}$		0.401	0.635	27 July 2020	6.15
$\alpha_{death,7}$		0.142	1.22	25 August 2020	4.51
$\alpha_{death,8}$		0.473	7.46	17 September 2020	1.20
$\alpha_{death,9}$		0.314	6.39	8 October 2020	1.56
$\alpha_{death,10}$		0.638	0.966	1 November 2020	2.18
$\alpha_{death,11}$		1.41	0.748	22 November 2020	1.17
$\alpha_{death,12}$		1.64	2.53	11 December 2020	1.89
$\alpha_{death,13}$		2.54	1.35	29 December 2020	0.499
$\alpha_{death,14}$		2.66	3.01	7 January 2021	6.02
$\alpha_{death,15}$		3.48	6.42	18 January 2021	1.43
$\alpha_{death,16}$		2.31	4.80	5 February 2021	0.794
$\alpha_{death,17}$		1.22	3.15	27 February 2021	2.315
$\alpha_{death,18}$		0.807	2.15	09 March 2021	3.75
$\alpha_{death,19}$		1.09	69.1	19 March 2021	-

Table A4. Residual errors of observables. We present the residual errors of fitting our model to the time frame 3 March 2020 to 21 March 2021. dIM = daily incident cases, IM = cumulative, dICU = daily occupation of ICU beds dD = daily death, D = cumulative delay. Case numbers were square root transformed, i.e., units of values are cases to the power of 0.5.

Parameter	Value for Germany	Value for Saxony
a_{dIM}	3.62	0.921
a_{IM}	5.69	1.03
a_{dICU}	1.19	0.442
a_{dD}	3.04	0.377
a_D	0.99	1.14

Table A5. Parameter estimates and comparison with average priors. We present estimated parameters of the SECIR model and initial conditions of control parameters and their respective standard errors for Germany. We also perform a formal comparison of estimates and expected priors using *t*-test.

Parameter	Description	Posterior Estimate	Relative Standard Error, %	Prior Value	<i>p</i> -Value
influx	Initial influx of infections into compartment <i>E</i> until first interventions	3171	3.12	-	-
r_1	Infection rate through asymptomatic subjects	1.19	0.582	-	-
r_3	Transit rate for compartment <i>E</i> (latent time)	0.272	0.0571	1/3	0.213

Table A5. Cont.

Parameter	Description	Posterior Estimate	Relative Standard Error, %	Prior Value	p-Value
r_4	Transit rate for asymptomatic sub-compartments	0.636	0.734	3/5	0.429
$r_{4,b}$	Rate of development of symptoms after infection	0.456	2.17	1/2.5	0.346
r_5	Transit rate for symptomatic sub-compartments	0.946	2.33	3/2.5	0.499
r_6	Rate of development of critical state after being symptomatic	0.186	0.405	1/5	0.457
r_7	Transit rate for critical state sub-compartment	0.159	0.336	3/17	0.402
r_8	Death rate of patients in critical sub-compartment 1	0.104	0.409	1/8	0.441
$rb_{1,2}$	Proportionality coefficient of intensifications/relaxations between b_1 and b_2	0.379	9.18	-	-
$P_{S,M}$	Fraction of reported cases	0.499	0.102	1/2	
$p_{crit} (p_{crit,0})$	Probability of becoming critical after developing symptoms (initial value)	0.0765	0.706	-	-
$p_{death} (p_{death,0})$	Probability of death after becoming critical (initial value)	0.119	1.24	-	-
$p_{death,S,0}$	Proportionality coefficient for evaluating probability of death after developing symptoms without becoming critical, see (A6)	0.587	8.04	-	-

Appendix J. Parameter Values for Saxony

Table A6. Time points of changes in infectivity and respective values for Saxony. We used fixed (known due to Governmental decisions or random events) and estimated time points of changes of NPI/contact behavior and events and respective changes in infectivity of asymptomatic subjects. We provide estimates and relative standard errors of the infectivity starting with the date mentioned (3 to 5 column).

Numbers	Type of NPI/ Behavior Change	Estimated New Infectivity	Relative Standard Error, %	Date	Source	Standard Error (Days)
1	Intensification	0.606	0.877	10 March 2020	Fixed	-
2	Intensification	0.120	5.41	15 March 2020	Fixed	-
3	Intensification	0.0904	1.15	22 March 2020	Fixed	-
4	Relaxation	0.103	1.98	2 April 2020	Estimated	0.541
5	Intensification	0.0907	3.12	14 April 2020	Estimated	0.237
6	Relaxation	0.302	0.965	30 April 2020	Fixed	-
7	Intensification	0.0606	6.08	7 May 2020	Fixed	-
8	Intensification	0.0385	4.21	14 May 2020	Fixed	-
9	Relaxation	0.0601	0.199	19 May 2020	Estimated	0.487
10	Relaxation	0.817	0.505	4 June 2020	Estimated	0.603
11	Intensification	0.0344	4.18	11 June 2020	Estimated	0.456
12	Relaxation	0.219	3.23	30 June 2020	Estimated	0.298

Table A6. Cont.

Numbers	Type of NPI/ Behavior Change	Estimated New Infectivity	Relative Standard Error, %	Date	Source	Standard Error (Days)
13	Intensification	0.149	1.13	16 August 2020	Estimated	0.312
14	Relaxation	0.213	2.29	26 August 2020	Estimated	0.578
15	Relaxation	0.297	0.78	4 October 2020	Estimated	0.209
16	Intensification	0.185	1.26	21 October 2020	Estimated	0.352
17	Intensification	0.152	5.93	30 October 2020	Fixed	-
18	Relaxation	0.201	0.826	11 November 2020	Estimated	1.21
19	Relaxation	0.207	0.652	19 November 2020	Estimated	0.318
20	Intensification	0.201	2.13	22 November 2020	Estimated	0.554
21	Intensification	0.0672	1.87	10 December 2020	Fixed	-
22	Relaxation	0.228	1.36	18 December 2020	Estimated	0.426
23	Intensification	0.0937	5.09	1 January 2021	Estimated	0.141
24	Relaxation	0.120	9.78	14 January 2021	Estimated	-
25	Relaxation	0.229	10.1	5 February 2021	Estimated	-
26	Intensification	0.150	11.5	15 February 2021	Estimated	-
27	Relaxation	0.199	0.95	26 February 2021	Estimated	-
28	Relaxation	0.210	25.7	18 March 2021	Fixed	-

Table A7. Step functions of p_{crit} and p_{death} for Saxony. We present estimates for the steps of the functions p_{crit} and p_{death} at the specified dates and respective standard errors for Saxony. We also provide the standard error of the estimated time point (last column).

Parameter	Description	Estimate	Relative Standard Error, %	Date Respective Controls	Standard Error (Days)
$\alpha_{crit,1}$	Relative values of p_{crit} starting at the respective date	2.15	0.98	24 March 2020	0.34
$\alpha_{crit,2}$		1.99	4.22	10 April 2020	0.672
$\alpha_{crit,3}$		1.01	3.54	11 May 2020	1.25
$\alpha_{crit,4}$		2.54	2.49	5 June 2020	3.73
$\alpha_{crit,5}$		1.50	1.26	2 July 2020	4.36
$\alpha_{crit,6}$		1.19	3.41	27 July 2020	0.75
$\alpha_{crit,7}$		0.764	0.478	29 August 2020	4.93
$\alpha_{crit,8}$		0.398	5.12	18 September 2020	2.96
$\alpha_{crit,9}$		0.300	2.09	25 September 2020	2.12
$\alpha_{crit,10}$		0.528	2.16	13 October 2020	0.49
$\alpha_{crit,11}$		0.908	3.72	26 October 2020	1.15
$\alpha_{crit,12}$		0.999	2.43	1 December 2020	5.31
$\alpha_{crit,13}$		1.76	1.91	26 December 2020	2.06
$\alpha_{crit,14}$		2.01	1.56	10 January 2021	0.67
$\alpha_{crit,15}$		2.99	0.98	25 January 2021	2.15
$\alpha_{crit,16}$		2.68	5.77	13 February 2021	4.12
$\alpha_{crit,17}$		1.11	1.33	5 March 2021	5.11
$\alpha_{crit,18}$		0.700	79.2	4 March 2021	-

Table A7. Cont.

Parameter	Description	Estimate	Relative Standard Error, %	Date Respective Controls	Standard Error (Days)
$\alpha_{death,1}$	Relative values of p_{death} starting at the respective date	0.655	2.26	4 April 2020	0.241
$\alpha_{death,2}$		3.58	6.81	24 April 2020	0.335
$\alpha_{death,3}$		1.94	5.32	17 May 2020	1.01
$\alpha_{death,4}$		0.743	1.07	8 June 2020	0.619
$\alpha_{death,5}$		0.296	4.32	7 July 2020	5.60
$\alpha_{death,6}$		0.401	1.56	4 August 2020	6.13
$\alpha_{death,7}$		0.142	6.77	26 August 2020	4.43
$\alpha_{death,8}$		0.473	9.05	27 September 2020	0.95
$\alpha_{death,9}$		0.314	1.42	3 October 2020	1.27
$\alpha_{death,10}$		0.638	0.84	2 November 2020	3.62
$\alpha_{death,11}$		1.41	0.9	16 November 2020	1.19
$\alpha_{death,12}$		1.64	2.31	1 December 2020	1.63
$\alpha_{death,13}$		2.54	1.555	20 December 2020	0.903
$\alpha_{death,14}$		2.66	3.89	8 January 2021	5.52
$\alpha_{death,15}$		3.48	5.53	19 January 2021	1.08
$\alpha_{death,16}$		2.31	4.9	09 February 2021	0.383
$\alpha_{death,17}$		1.22	2.76	26 February 2021	2.06
$\alpha_{death,18}$		0.807	4.03	7 March 2021	5.34
$\alpha_{death,19}$		1.09	70.1	11 March 2021	-

Table A8. Parameter estimates and comparison with average priors for the parameter settings for Saxony. We present estimated parameters of the SECIR model and initial conditions of control parameters and their respective standard errors for the parametrization of the epidemic in Saxony. We also perform a formal comparison of estimates and expected priors using t -test.

Parameter	Description	Posterior Estimate	Relative Standard Error, %	Prior Value	p -Value
influx	Initial influx of infections into compartment E until first interventions	68.1	6.17	-	-
r_1	Infection rate through asymptomatic subjects	1.61	1.32	-	-
r_3	Transit rate for compartment E (latent time)	0.270	0.234	1/3	0.221
r_4	Transit rate for asymptomatic sub-compartments	0.697	0.691	3/5	0.357
$r_{4,b}$	Rate of development of symptoms after infection	0.294	3.27	1/2.5	0.489
r_5	Transit rate for symptomatic sub-compartments	1.11	2.13	3/2.5	0.236
r_6	Rate of development of critical state after being symptomatic	0.170	1.46	1/5	0.495
r_7	Transit rate for critical state sub-compartment	0.198	0.659	3/17	0.372

Table A8. Cont.

Parameter	Description	Posterior Estimate	Relative Standard Error, %	Prior Value	p-Value
r_8	Death rate of patients in critical sub-compartment 1	0.140	1.33	1/8	0.393
$rb_{1,2}$	Proportional coefficient of intensifications/relaxations between b_1 and b_2	0.248	15.5	-	-
$P_{S,M}$	Fraction of reported cases	0.509	5.37	1/2	
p_{crit} ($p_{crit,0}$)	Probability of becoming critical after developing symptoms (initial value)	0.0794	1.76	-	-
p_{death} ($p_{death,0}$)	Probability of death after becoming critical (initial value)	0.137	0.957	-	-
$P_{death,S,0}$	Proportionality coefficient for evaluating probability of death after developing symptoms without becoming critical, see (A6)	0.719	7.3	-	-

References

- Adiga, A.; Dubhashi, D.; Lewis, B.; Marathe, M.; Venkatramanan, S.; Vullikanti, A. Mathematical Models for COVID-19 Pandemic: A Comparative Analysis. *J. Indian Inst. Sci.* **2020**, *100*, 793–807. [[CrossRef](#)]
- Tang, J.; Vinayavekhin, S.; Weeramongkolkul, M.; Suksanon, C.; Pattarapremcharoen, K.; Thiwathittayanuphap, S.; Leelawat, N. Agent-Based Simulation and Modeling of COVID-19 Pandemic: A Bibliometric Analysis. *J. Disaster Res.* **2022**, *17*, 93–102. [[CrossRef](#)]
- Kucharski, A.J.; Klepac, P.; Conlan, A.J.K.; Kissler, S.M.; Tang, M.L.; Fry, H.; Gog, J.R.; Edmunds, W.J.; Emery, J.C.; Medley, G.; et al. Effectiveness of isolation, testing, contact tracing, and physical distancing on reducing transmission of SARS-CoV-2 in different settings: A mathematical modelling study. *Lancet Infect. Dis.* **2020**, *20*, 1151–1160. [[CrossRef](#)]
- Quilty, B.J.; Clifford, S.; Hellewell, J.; Russell, T.W.; Kucharski, A.J.; Flasche, S.; Edmunds, W.J.; E Atkins, K.; Foss, A.M.; Waterlow, N.R.; et al. Quarantine and testing strategies in contact tracing for SARS-CoV-2: A modelling study. *Lancet Public Health* **2021**, *6*, e175–e183. [[CrossRef](#)]
- Rahimi, I.; Chen, F.; Gandomi, A.H. A review on COVID-19 forecasting models. *Neural Comput. Appl.* **2021**. [[CrossRef](#)]
- Flaxman, S.; Mishra, S.; Gandy, A.; Unwin, H.J.T.; Mellan, T.A.; Coupland, H.; Whittaker, C.; Zhu, H.; Berah, T.; Eaton, J.W.; et al. Estimating the effects of non-pharmaceutical interventions on COVID-19 in Europe. *Nature* **2020**, *584*, 257–261. [[CrossRef](#)]
- Bo, Y.; Guo, C.; Lin, C.; Zeng, Y.; Li, H.B.; Zhang, Y.; Hossain, S.; Chan, J.W.; Yeung, D.W.; Kwok, K.O.; et al. Effectiveness of non-pharmaceutical interventions on COVID-19 transmission in 190 countries from 23 January to 13 April 2020. *Int. J. Infect. Dis.* **2020**, *102*, 247–253. [[CrossRef](#)]
- Khailaie, S.; Mitra, T.; Bandyopadhyay, A.; Schips, M.; Mascheroni, P.; Vanella, P.; Lange, B.; Binder, S.C.; Meyer-Hermann, M. Development of the reproduction number from coronavirus SARS-CoV-2 case data in Germany and implications for political measures. *BMC Med.* **2020**, *19*, 32. [[CrossRef](#)]
- Barbarossa, M.V.; Fuhrmann, J.; Meinke, J.H.; Krieg, S.; Varma, H.V.; Castelletti, N.; Lippert, T. Modeling the spread of COVID-19 in Germany: Early assessment and possible scenarios. *PLoS ONE* **2020**, *15*, e0238559. [[CrossRef](#)]
- der Heiden, M.; an Buchholz, U. *Modellierung von Beispielszenarien der SARS-CoV-2-Epidemie 2020 in Deutschland*; Robert Koch-Institut: Berlin, Germany, 2020.
- Dehning, J.; Zierenberg, J.; Spitzner, F.P.; Wibral, M.; Neto, J.P.; Wilczek, M.; Priesemann, V. Inferring change points in the spread of COVID-19 reveals the effectiveness of interventions. *Science* **2020**, *369*, eabb9789. [[CrossRef](#)]
- Harris, J.E. Overcoming Reporting Delays Is Critical to Timely Epidemic Monitoring: The Case of COVID-19 in New York City. *MedRxiv* **2020**. [[CrossRef](#)]
- Böttcher, S.; Oh, D.-Y.; Staat, D.; Stern, D.; Albrecht, S.; Wilrich, N.; Zacher, B.; Mielke, M.; Rexroth, U.; Hamouda, O. *Erfassung der SARS-CoV-2-Testzahlen in Deutschland (Stand 2.12.2020)*; Robert Koch-Institut: Berlin, Germany, 2020.
- McCulloh, I.; Kiernan, K.; Kent, T. Improved Estimation of Daily COVID-19 Rate from Incomplete Data. In Proceedings of the 2020 Fourth International Conference on Multimedia Computing, Networking and Applications (MCNA), Valencia, Spain, 19–22 October 2020; pp. 153–158.
- Ram, V.; Schaposnik, L.P. A modified age-structured SIR model for COVID-19 type viruses. *Sci. Rep.* **2021**, *11*, 15194. [[CrossRef](#)] [[PubMed](#)]
- Cooper, I.; Mondal, A.; Antonopoulos, C.G. A SIR model assumption for the spread of COVID-19 in different communities. *Chaos Solitons Fractals* **2020**, *139*, 110057. [[CrossRef](#)] [[PubMed](#)]

17. Georgatzis, K.; Williams, C.K.I.; Hawthorne, C. Input-Output Non-Linear Dynamical Systems applied to Physiological Condition Monitoring. In Proceedings of the 1st Machine Learning for Healthcare Conference 2016: PMLR, Los Angeles, CA, USA, 19–20 August 2016.
18. Nishiura, H.; Linton, N.M.; Akhmetzhanov, A.R. Serial interval of novel coronavirus (COVID-19) infections. *Int. J. Infect. Dis.* **2020**, *93*, 284–286. [[CrossRef](#)]
19. Tindale, L.C.; E Stockdale, J.; Coombe, M.; Garlock, E.S.; Lau, W.Y.V.; Saraswat, M.; Zhang, L.; Chen, D.; Wallinga, J.; Colijn, C. Evidence for transmission of COVID-19 prior to symptom onset. *eLife* **2020**, *9*, e57149. [[CrossRef](#)]
20. Böhmer, M.M.; Buchholz, U.; Corman, V.M.; Hoch, M.; Katz, K.; Marosevic, D.V.; Böhm, S.; Woudenberg, T.; Ackermann, N.; Konrad, R.; et al. Investigation of a COVID-19 outbreak in Germany resulting from a single travel-associated primary case: A case series. *Lancet Infect. Dis.* **2020**, *20*, 920–928. [[CrossRef](#)]
21. Ganyani, T.; Kremer, C.; Chen, D.; Torneri, A.; Faes, C.; Wallinga, J.; Hens, N. Estimating the generation interval for coronavirus disease (COVID-19) based on symptom onset data, March 2020. *Eurosurveillance* **2020**, *25*, 2000257. [[CrossRef](#)]
22. Wölfel, R.; Corman, V.M.; Guggemos, W.; Seilmaier, M.; Zange, S.; Müller, M.A.; Niemeyer, D.; Jones, T.C.; Vollmar, P.; Rothe, C.; et al. Virological assessment of hospitalized patients with COVID-2019. *Nature* **2020**, *581*, 465–469. [[CrossRef](#)]
23. Hu, Z.; Song, C.; Xu, C.; Jin, G.; Chen, Y.; Xu, X.; Ma, H.; Chen, W.; Lin, Y.; Zheng, Y.; et al. Clinical characteristics of 24 asymptomatic infections with COVID-19 screened among close contacts in Nanjing, China. *Sci. China Life Sci.* **2020**, *63*, 706–711. [[CrossRef](#)]
24. Li, R.; Pei, S.; Chen, B.; Song, Y.; Zhang, T.; Yang, W.; Shaman, J. Substantial undocumented infection facilitates the rapid dissemination of novel coronavirus (SARS-CoV-2). *Science* **2020**, *368*, 489–493. [[CrossRef](#)]
25. Stebbeg, M.; Kumar, S.D.; Silva-Cayetano, A.; Fonseca, V.R.; Linterman, M.A.; Graca, L. Regulation of the Germinal Center Response. *Front. Immunol.* **2018**, *9*, 2469. [[CrossRef](#)] [[PubMed](#)]
26. Hao, X.; Cheng, S.; Wu, D.; Wu, T.; Lin, X.; Wang, C. Reconstruction of the full transmission dynamics of COVID-19 in Wuhan. *Nature* **2020**, *584*, 420–424. [[CrossRef](#)] [[PubMed](#)]
27. He, X.; Lau, E.H.Y.; Wu, P.; Deng, X.; Wang, J.; Hao, X.; Lau, Y.C.; Wong, J.Y.; Guan, Y.; Tan, X.; et al. Temporal dynamics in viral shedding and transmissibility of COVID-19. *Nat. Med.* **2020**, *26*, 672–675. [[CrossRef](#)]
28. Epidemiologischer Steckbrief zu SARS-CoV-2 und COVID-19. RKI 2021. Available online: https://www.rki.de/DE/Content/InfAZ/N/Neuartiges_Coronavirus/Steckbrief.html#ses- (accessed on 26 November 2021).
29. Zhou, F.; Yu, T.; Du, R.; Fan, G.; Liu, Y.; Liu, Z.; Xiang, J.; Wang, Y.; Song, B.; Gu, X.; et al. Clinical course and risk factors for mortality of adult inpatients with COVID-19 in Wuhan, China: A retrospective cohort study. *Lancet* **2020**, *395*, 1054–1062. [[CrossRef](#)]
30. Sanche, S.; Lin, Y.T.; Xu, C.; Romero-Severson, E.; Hengartner, N.; Ke, R. High Contagiousness and Rapid Spread of Severe Acute Respiratory Syndrome Coronavirus 2. *Emerg. Infect. Dis.* **2020**, *26*, 1470–1477. [[CrossRef](#)]
31. COVID-19 National Emergency Response Center. Coronavirus Disease-19: The First 7755 Cases in the Republic of Korea. *Osong Public Health Res. Perspect* **2020**, *11*, 85–90. [[CrossRef](#)]
32. Schuppert, A.; Theisen, S.; Fränkel, P.; Weber-Carstens, S.; Karagiannidis, C. Bundesweites Belastungsmodell für Intensivstationen durch COVID-19. *Med. Klin.-Intensivmed. Und Notf.* **2022**, *117*, 218–226. [[CrossRef](#)]
33. Tolksdorf, K.; Buda, S.; Schuler, E.; Wieler, L.H.; Haas, W. Eine höhere Letalität und lange Beatmungsdauer unterscheiden COVID-19 von schwer verlaufenden Atemwegsinfektionen in Grippewellen. *Epidemiol. Bull.* **2020**, *41*. [[CrossRef](#)]
34. Karagiannidis, C.; Mostert, C.; Hentschker, C.; Voshaar, T.; Malzahn, J.; Schillinger, G.; Klauber, J.; Janssens, U.; Marx, G.; Weber-Carstens, S.; et al. Case characteristics, resource use, and outcomes of 10,021 patients with COVID-19 admitted to 920 German hospitals: An observational study. *Lancet Respir. Med.* **2020**, *8*, 853–862. [[CrossRef](#)]
35. Verity, R.; Okell, L.C.; Dorigatti, I.; Winskill, P.; Whittaker, C.; Imai, N.; Guomo-Dannenburg, G.; Thompson, H.; Walker, P.G.T.; Fu, H.; et al. Estimates of the severity of coronavirus disease 2019: A model-based analysis. *Lancet Infectious Dis.* **2020**, *20*, 669–677. [[CrossRef](#)]
36. Linton, N.; Kobayashi, T.; Yang, Y.; Hayashi, K.; Akhmetzhanov, A.; Jung, S.-M.; Yuan, B.; Kinoshita, R.; Nishiura, H. Incubation Period and Other Epidemiological Characteristics of 2019 Novel Coronavirus Infections with Right Truncation: A Statistical Analysis of Publicly Available Case Data. *J. Clin. Med.* **2020**, *9*, 538. [[CrossRef](#)] [[PubMed](#)]
37. Byambasuren, O.; Cardona, M.; Bell, K.; Clark, J.; McLaws, M.-L.; Glasziou, P. Estimating the extent of asymptomatic COVID-19 and its potential for community transmission: Systematic review and meta-analysis. *J. Assoc. Med. Microbiol. Infect. Dis.* **2020**, *5*, 223–234. [[CrossRef](#)]
38. Oran, D.P.; Topol, E.J. Prevalence of Asymptomatic SARS-CoV-2 Infection: A Narrative Review. *Ann. Intern. Med.* **2020**, *173*, 362–367. [[CrossRef](#)] [[PubMed](#)]
39. Buitrago-Garcia, D.; Egli-Gany, D.; Counotte, M.J.; Hossmann, S.; Imeri, H.; Ipekci, A.M.; Salanti, G.; Low, N. Occurrence and transmission potential of asymptomatic and presymptomatic SARS-CoV-2 infections: A living systematic review and meta-analysis. *PLoS Med.* **2020**, *17*, e1003346. [[CrossRef](#)]
40. Neuhauser, H.; Thamm, R.; Buttman-Schweiger, N.; Fiebig, J.; Offergeld, R.; Poethko-Müller, C.; Prütz, F.; Santos-Hövenner, C.; Sarganas, G.; Angelika, S.R.; et al. Ergebnisse seroepidemiologischer Studien zu SARS-CoV-2 in Stichproben der Allgemeinbevölkerung und bei Blutspenderinnen und Blutspendern in Deutschland (Stand 03.12.2020). *Epidemiol. Bull.* **2020**, *50*. [[CrossRef](#)]

41. Gornyk, D.; Harries, M.; Glöckner, S.; Strengert, M.; Kerrinnes, T.; Bojara, G.; Krause, G. SARS-CoV-2 seroprevalence in Germany—A population based sequential study in five regions. *medRxiv* **2021**. [CrossRef]
42. Bock, W.; Jayathunga, Y.; Götz, T.; Rockenfeller, R. Are the upper bounds for new SARS-CoV-2 infections in Germany useful. *Comput. Math. Biophys.* **2021**, *9*, 242–260. [CrossRef]
43. COVID-19-Fälle nach Meldewoche und Geschlecht sowie Anteile mit für COVID-19 relevanten Symptomen, Anteile Hospitalisierter/Verstorbener und Altersmittelwert/-median (Tabelle wird jeden Donnerstag aktualisiert). RKI 2020. Available online: https://www.rki.de/DE/Content/InfAZ/N/Neuartiges_Coronavirus/Daten/Klinische_Aspekte.html (accessed on 26 June 2022).
44. Tagesreport-Archiv. DIVI 2020. Available online: <https://www.divi.de/divi-intensivregister-tagesreport-> (accessed on 26 June 2022).
45. Delgado, G.; Safranek, J.; Goyette, B.; Spady, R. Reported versus Actual Date of Death. “Reported” versus “Actual”: Two Different Things. Available online: <https://covidplanningtools.com/reported-versus-actual-date-of-death/> (accessed on 26 June 2022).
46. Robert Koch Institute. Bericht zu Virusvarianten von SARS-CoV-2 in Deutschland, insbesondere zur Variant of Concern (VOC) B.1.1.7. Available online: https://www.rki.de/DE/Content/InfAZ/N/Neuartiges_Coronavirus/DESH/Bericht_VOC_2021-03-03.pdf?__blob=publicationFile (accessed on 3 March 2021).
47. Kheifetz, Y.; Scholz, M. Modeling individual time courses of thrombopoiesis during multi-cyclic chemotherapy. *PLoS Comput. Biol.* **2019**, *15*, e1006775. [CrossRef]
48. Kuhn, E.; Lavielle, M. Coupling a stochastic approximation version of EM with an MCMC procedure. *ESAIM Probab. Stat.* **2004**, *8*, 115–131. [CrossRef]
49. Meineke, F.A.; Löbe, M.; Stäubert, S. Introducing Technical Aspects of Research Data Management in the Leipzig Health Atlas. *Stud. Health Technol. Inform.* **2018**, *247*, 426–430.
50. Hale, T.; Angrist, N.; Goldszmidt, R.; Kira, B.; Petherick, A.; Phillips, T.; Webster, S.; Cameron-Blake, E.; Hallas, L.; Majumdar, S.; et al. A global panel database of pandemic policies (Oxford COVID-19 Government Response Tracker). *Nat. Hum. Behav.* **2021**, *5*, 529–538. [CrossRef] [PubMed]
51. COVID-19 Government Response Tracker; University of Oxford: Oxford, UK, 2020. Available online: <https://www.bsg.ox.ac.uk/research/research-projects/covid-19-government-response-tracker> (accessed on 3 March 2022).
52. Mullen, J.L.; Tsueng, G.; Latif, A.A.; Alkuzweny, M.; Cano, M.; Haag, E.; Zhou, J.; Zeller, M.; Hufbauer, E.; Matteson, N. Outbreak.info. A Standardized, Open-Source Database of COVID-19 Resources and Epidemiology Data. Available online: <https://outbreak.info> (accessed on 18 July 2021).
53. Aktuelle Entwicklung der COVID-19 Epidemie in Leipzig und Sachsen. Bulletin 14 vom 20.02.2021. Available online: https://www.imise.uni-leipzig.de/sites/www.imise.uni-leipzig.de/files/files/uploads/Medien/bulletin_n14_covid19_sachsen_2021_02_22_v11.pdf (accessed on 26 June 2022).
54. Scholz, S.; Waize, M.; Weidemann, F.; Treskova-Schwarzbach, M.; Haas, L.; Harder, T.; Karch, A.; Lange, B.; Kuhlmann, A.; Jäger, V.; et al. Einfluss von Impfungen und Kontaktreduktionen auf die dritte Welle der SARS-CoV-2-Pandemie und perspektivische Rückkehr zu prä-pandemischem Kontaktverhalten. 2021. Available online: <https://edoc.rki.de/handle/176904/8023?show=full> (accessed on 26 June 2022).
55. Friberg, L.E.; Henningson, A.; Maas, H.; Nguyen, L.; Karlsson, M.O. Model of chemotherapy-induced myelosuppression with parameter consistency across drugs. *J. Clin. Oncol.* **2002**, *20*, 4713–4721. [CrossRef] [PubMed]
56. Maire, F.; Friel, N.; Mira, A.; Raftery, A.E. Adaptive Incremental Mixture Markov Chain Monte Carlo. *J. Comput. Graph. Stat.* **2019**, *28*, 790–805. [CrossRef]
57. Bracher, J.; Wolfram, D.; Deuschel, J.; Görgen, K.; Ketterer, J.L.; Ullrich, A.; Abbott, S.; Barbarossa, M.V.; Bertsimas, D.; Bhatia, S.; et al. A pre-registered short-term forecasting study of COVID-19 in Germany and Poland during the second wave. *Nat. Commun.* **2021**, *12*, 5173. [CrossRef]
58. Dempster, A.P.; Laird, N.M.; Rubin, D.B. Maximum Likelihood from Incomplete Data Via the EM Algorithm. *J. R. Stat. Soc. Ser. B Methodol.* **1977**, *39*, 1–22. [CrossRef]
59. Tierney, L. Markov Chains for Exploring Posterior Distributions. *Ann. Stat.* **1994**, *22*, 1701–1728. [CrossRef]
60. Haario, H.; Saksman, E.; Tamminen, J. An Adaptive Metropolis Algorithm. *Bernoulli* **2001**, *7*, 223. [CrossRef]
61. Geweke, J.F. Evaluating the Accuracy of Sampling-Based Approaches to the Calculation of Posterior Moments. In *Bayesian Statistics*; Bernardo, J.M., Berger, J.O., Dawid, A.P., Smith, A.F.M., Eds.; Clarendon Press: Oxford, UK, 1992; p. 4.
62. Wu, Z.; McGoogan, J.M. Characteristics of and Important Lessons From the Coronavirus Disease 2019 (COVID-19) Outbreak in China: Summary of a Report of 72 314 Cases From the Chinese Center for Disease Control and Prevention. *JAMA* **2020**, *323*, 1239–1242. [CrossRef]